On the chemical and spectro-photometric evolution of nearby galaxies

van den Hoek, L.B.

Publication date
1997

6

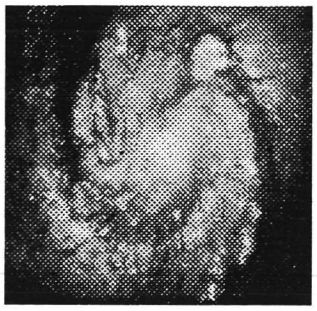

Modelling the spectro-photometric and chemical properties of Low Surface Brightness galaxies

van den Hoek, L.B., de Blok, W.J.G., van der Hulst, J.M., and de Jong, T.

Abstract

We investigate the star formation history and chemical evolution of low surface brightness (LSB) disk galaxies by means of their observed spectro-photometric and chemical properties. To this end, we use a galactic chemical evolution model incorporating a detailed metallicity dependent set of up-to-date stellar input data covering all relevant stages of stellar evolution. Comparison of our model results with observations confirms the idea that LSB galaxies are relatively unevolved systems.

Based on extensive modelling, we find that for the majority of the LSB galaxies in our sample, observed Johnson-Cousins UBVRI magnitudes, [O/H] abundances, gas masses and fractions, and HI mass-to-light ratios, are best explained by galactic evolution models incorporating an exponentially decreasing global star formation rate (SFR) ending at a present-day gas-to-total mass ratio of $\mu_1 = 0.5$ for a galaxy age of 14 Gyr. About 35 % of the LSB galaxies in our sample exhibit properties that cannot be explained by exponentially decreasing SFRs alone. We argue that most of these systems experienced recent episodes of enhanced star formation superimposed on exponentially decreasing global SFR models. Only a small fraction ($\sim$10$-$15 %) of the LSB galaxies have properties consistent with those resulting from linearly decreasing or constant SFR models.

We find evidence, from model point of view, for recent and ongoing star formation in the disks of LSB galaxies at rates of $\sim$0.1 $M_\odot$ yr^{-1}. In particular, we demonstrate that the occurrence of small amplitude star formation bursts in LSB galaxies is required to explain the contribution of the young (5-50 Myr old) stellar population to the galaxy integrated luminosity. This result suggests that star formation in LSB galaxies has proceeded in a stochastic manner from the moment star formation started in their disks. We argue that sporadic star formation in LSB galaxies is probably associated with *local* accretion and/or infall of matter.

The presence of an old stellar population in many late-type LSB galaxies, as confirmed by our results, suggests that LSB galaxies roughly follow the same evolutionary history as HSB galaxies, *except at a much lower rate*. In particular, our results imply that LSB galaxies do not form late, or have a delayed onset of star formation, but evolve slowly. We show that the observed color differences between LSB and HSB galaxies can be interpreted almost entirely in terms of the relatively low extinction and metallicity in LSB galaxies. We propose that LSB galaxies are in an early stage of disk formation and probably are still in the accumulation phase of gas during which their current amount of star formation and chemical enrichment is regulated. In particular, the gas reservoir at the time of onset of main star formation in LSB galaxies may have been substantially less than that estimated from their present-day amounts of gas since accretion of matter is still very important in these systems.

The low evolutionary state of LSB galaxies relative to HSB galaxies suggests that LSB galaxies are just HSB galaxies in the making (except on time scales much longer than a Hubble time). We discuss our results in the context of the evolutionary history of LSB galaxies compared to that of HSB and dwarf irregular galaxies.

6.1 Introduction

Deep searches for field galaxies in the local universe have revealed the existence of a large number of galaxies with such low surface brightnesses that they, until recently, were hard to detect against the night sky (Schombert et al. 1988, 1992; Knezek 1993; Turner et al. 1993; Bergvall & Rönnback 1995; Schwartzenberg et

al. 1995; Sprayberry et al. 1995). The low surface brightness galaxies detected in the field are predominantly late-type spirals which in general are disk-dominated, do not show any clear signs of a large bulge or strong bar, and have central surface brightnesses $\gtrsim 23$ mag arcsec^{-2} in the B band (e.g. Rönnback & Bergvall 1994; McGaugh & Bothun 1994; de Blok et al. 1995, hereafter dB95; Vennik et al. 1996). A small fraction (~ 15 %) of the field LSB galaxies detected thus far comprises early type systems, ellipticals, and dwarf galaxies.

The sizes and luminosities of LSB galaxies can range from the small and faint Local Group dwarfs like GR8 (Hodge 1967) to that of the giant and luminous Malin-1 like systems (e.g. Impey & Bothun 1989; Knezek 1993; Sprayberry et al. 1995). This latter group of giant LSB galaxies, which comprises ~ 10 % of the LSB galaxy population, usually have a large bulge and are much different from the disk dominated LSB galaxies described above.

In this paper, we will concentrate on late-type LSB spirals. The main property which distinguishes these systems from their "normal" late-type spirals is their low surface brightness, not e.g. their luminosity or optical size. Observations show that LSB galaxies are neither dwarf systems nor just the fainter counterparts of HSB spirals (de Blok et al. 1996, hereafter dB96).

In many cases, LSB galaxies follow the trends in galaxy properties found along the Hubble sequence towards very late types. These trends, including increasingly blue colors (e.g. Rönnback 1993; McGaugh & Bothun 1994; dB95), decreasing oxygen abundances in the gas (e.g. McGaugh 1994; Rönnback & Bergvall 1995), and decreasing HI surface densities (from type Sc onwards; e.g. van der Hulst et al. 1993, hereafter vdH93) suggest that LSB galaxies must be in a low evolutionary state compared to HSB galaxies.

Atomic gas surface densities of LSB spirals are among the lowest known for disk galaxies (dB96). Notwithstanding, LSB spirals rank among the most gas-rich disk galaxies of a given total mass as their HI disks in general are rather extended (Zwaan et al. 1995; dB96). The fact that LSB galaxies still have large reservoirs of gas together with their low abundances suggest that their amount of star formation in the past cannot have been very large. Clearly, LSB galaxies are not the faded remnants of HSB spirals.

Current star formation rates in LSB galaxies are among the lowest known for late-type disk galaxies as well, as deduced from narrow-band Hα imaging (McGaugh 1992; vdH93). These observations reveal the presence of a few giant HII regions which are ionized by OB associations formed during recent episodes of star formation (e.g. McGaugh 1992). Such sites of minimal star formation are, however, low in number, do not trace the spiral arms very well, and are usually found towards the outer parts of the galaxy (dB95). This suggests that *local* rather than *global* star formation is a common phenomenon in LSB galaxies.

The unevolved nature of LSB spirals as implied by their low gas abundances, unusually blue colors, low gas surface densities, large gas contents, and low current star formation rates, can be interpreted in many different ways. For instance, LSB spirals may be relatively young systems in which the main phase of star formation is still to occur. If the mean age of the stellar population in LSB galaxies is much younger than that in HSB spirals, this would imply different star formation histories for galaxies differing in surface brightness. Alternatively, the stellar population in LSB spirals might be as old as in their HSB counterparts but with a young population dominating the luminosity. This would imply similar star formation histories and further would suggest the existence of a distinct group of red LSB spirals undetected yet because of their absence of a young stellar population (e.g. McGaugh & Bothun 1994). Other explanations for the dissimilarities observed between LSB and HSB spirals may include differences in internal extinction and/or in the stellar mass function at birth.

The goal of this paper is to address these and other scenarios for the evolution of LSB galaxies by detailed modelling of their spectro-photometric and chemical properties. The model used incorporates a detailed metallicity dependent set of stellar input data covering all relevant stages of stellar evolution and is able to describe the evolution of low metallicity galaxies such as LSB spirals.

Model results are compared directly with the observed colors, gas phase abundances, gas contents, and current star formation rates of LSB galaxies to constrain the global star formation history and chemical evolution of these systems. In particular, we consider the important question whether LSB spirals do have an evolutionary history fundamentally different from that of HSB spirals and dwarf galaxies. We will show that models incorporating exponentially decreasing SFRs are in best agreement with the spectro-photometric and chemical properties of the majority of the LSB galaxies in our sample, provided that these LSB galaxies have turned about half of their present-day disk mass into stars.

This paper is organized as follows. We briefly compare observational data of LSB galaxies with those of face-on spirals and dwarf galaxies in Sect. 6.2. In Sect. 6.3, we describe the ingredients of the galactic evolution model developed to study the spectro-photometric evolution of LSB spirals. In Sect. 6.4, we compare and calibrate the model and describe the initial set of star formation histories studied. Model

results related to the chemical and spectro-photometric evolution of LSB galaxies are presented in Sect. 6.5. The impact of small amplitude star formation bursts in LSB galaxies is investigated in Sect. 6 and predicted star formation rates are compared with the observations in Sect. 6.7. We discuss our results in the context of the star formation history and dynamical evolution of LSB galaxies in Sect. 6.8.

6.2 Observational characteristics of LSB galaxies

To amplify the properties of LSB galaxies, we compare Johnson-Cousins UBVRI magnitudes, neutral hydrogen masses, gas fractions, and oxygen abundances of LSB galaxies, with those of HSB and dwarf galaxies.

6.2.1 Sample selection

We refer to de Blok et al. (1996) for an extensive description of the sample selection. In brief, their sample consists of 24 late-type LSB galaxies (inclinations up to $\sim 60^o$), taken from the lists by Schombert et al. (1992) and the UGC (Nilson 1973), which are representative for the LSB galaxies generally found in the field by Schombert et al. For these systems, optical data have been taken from dB95, HI data from dB96, and abundance data from McGaugh & Bothun (1994) and de Blok & van der Hulst (unpublished).

From this sample, we selected a subsample of 16 LSB galaxies for which high-quality data are available. We list the galaxy identification and UBVRI absolute magnitudes in columns (1) to (6) in Table 6.1 (a Hubble constant of $H_0 = 100$ km s^{-1} Mpc^{-1} was used). To allow for direct comparison with photometric evolution models Johnson UBV and Kron-Cousins RI magnitudes will be used throughout this paper. Corresponding luminosities and mass-to-light ratios in the B band, neutral hydrogen and dynamical masses, gas-to-total mass ratios μ (corrected for helium; see Sect. 2.6 for the definition of $\mu_{\rm dyn}$ and $\mu_{\rm rot}$), and mean [O/H] abundances are listed in columns (7) to (13).

In addition to the sample listed in Table 6.1, we consider a complementary set of LSB galaxies for which less data are available. For these systems, we use photometry data presented by McGaugh et al. (1995) and abundance data provided by McGaugh (1994) and Rönnback & Bergvall (1994). Selection criteria for the McGaugh et al. (1995) sample were the same as those used by dB95. The LSB galaxies from Rönnback & Bergvall (1994) were selected in a different manner. In general, both sets of complementary LSB galaxies show properties similar to those of the dB95 subsample.

Table 6.1 Observational data on LSB galaxies (de Blok et al. 1995, 1996)

(1) Name	(2) U mag	(3) B mag	(4) V mag	(5) R mag	(6) I mag	(7) L_B [$L_{\odot,B}$]	(8) $M_{HI}\ L_B^{-1}$ [$M_\odot\ L_{\odot,B}^{-1}$]	(9) M_{HI} [$M_\odot$]	(10) M_{dyn} [$M_\odot$]	(11) μ_{dyn}	(12) μ_{rot}	(13) [O/H]
F561-1	-17.4	-17.2	-17.8	-18.0	-18.4	1.2(9)	0.7	8.1(8)	4.6(9)	0.24	0.59	-0.87
F563-1	-16.6	-16.7	-17.4	-17.6	-16.4†	7.4(8)	2.0	1.5(9)	3.8(10)	0.05	0.19	-1.46
F563-V1	-15.7	-15.7	-16.3	-16.6†	-16.9	3.0(8)	0.9	2.8(8)	1.0(9)	0.38	0.59	-1.05
F564-V3	*	-11.8	-12.4	-12.6	*	8.2(6)	1.6	1.3(7)	6.3(8)	0.03	*	*
F565-V2	*	-14.8	-15.3	-15.6	*	1.3(8)	2.6	3.4(8)	3.8(9)	0.12	0.33	*
F567-2	-17.0	-16.8	-17.4	-17.4	-17.7	8.2(8)	1.5	1.2(9)	8.1(9)	0.20	0.49	*
F568-1	-17.7	-17.5	-18.1	-18.3	-18.8	1.6(9)	1.4	2.2(9)	3.6(10)	0.08	0.32	-0.98
F568-3	-17.8	-17.7	-18.2	-18.5	-19.0	1.9(9)	0.8	1.6(9)	4.2(10)	0.05	0.45	-0.92
F568-V1	-17.4	-17.3	-17.8	-18.0	-18.5	1.3(9)	1.1	1.4(9)	5.1(10)†	0.04	0.53	-0.99
F571-5	-16.6	-16.5	-16.9	-17.1	*	6.2(8)	*	9.8(9)†	2.8(10)	0.47	*	-1.53
F571-V1	*	-16.4	-16.9	-17.3	*	5.6(8)	1.2	6.6(8)	1.4(10)	0.07	0.33	-0.94
F574-2	*	-17.0	-17.7	-17.8	*	9.8(8)	0.9	9.3(8)	3.2(9)	0.39	0.66	*
F577-V1	-17.9	-17.6	-18.0	-18.1	*	1.7(9)	0.8	1.4(9)	1.6(9)†	∼1.	*	*
U0128	-18.5	-18.2	-18.7	-18.9	-19.3	3.0(9)	1.2	3.6(9)	7.2(10)	0.07	0.39	*
U0628	-18.5	-18.5	-19.1	-19.3	-19.7	3.9(9)	*	*	4.9(10)	*	*	*
U1230	-18.9	-17.7	-18.2	-18.5	-18.9	1.9(9)	1.7	3.2(9)	6.3(10)	0.05	0.60	-0.76
Typ. Dwarf	-17.5	-17	-17.5	-18	-18.5	1.0(9)	1.0	1(9)	1(9)	0.5	*	−0.6±0.4
Typ. LSBG	-18	-17.5	-18	-18	-18.5	1.5(9)	1.3	2(9)	1(10)	0.2	0.5	−0.6±0.4
Typ. HSBG	-20	-19.5	-20	-20.5	-21	1.0(10)	0.4	4(9)	1(11)	0.04	*	∼0.0

* not available, † uncertain

6.2.2 Magnitudes and colors

We compare in Fig. 6.1 magnitudes and broadband colors of LSB galaxies to those of HSB face-on spirals (de Jong & van der Kruit 1994) and dwarf galaxies (Melisse & Israel 1994; Gallagher & Hunter 1986, 1987). We note that the usual distinction between HSB and LSB galaxies is purely an artificial one since normal

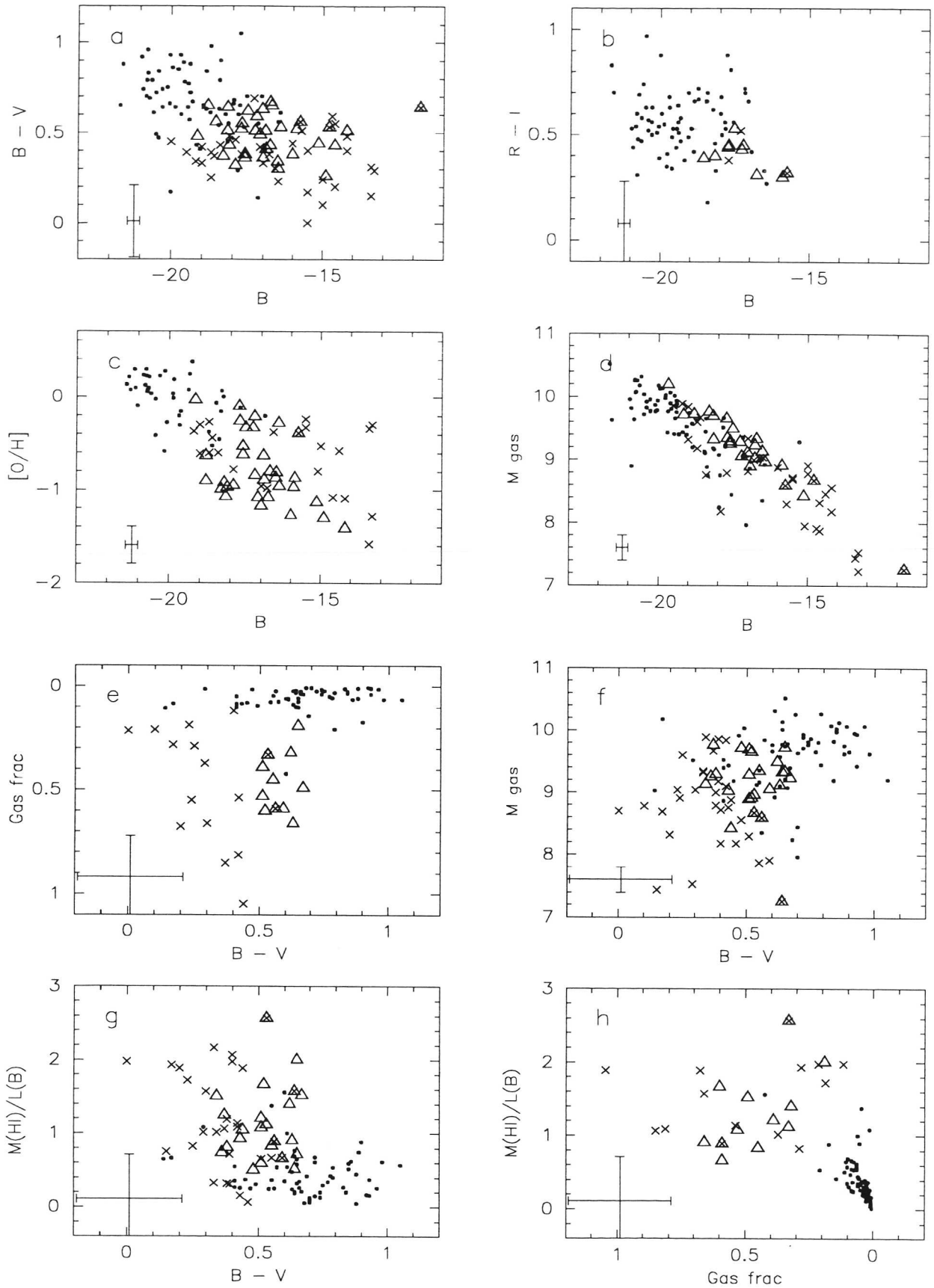

Figure 6.1 Observational data on LSB galaxies compared to that for normal spirals and dwarf galaxies. Symbols refer to LSB galaxies (triangles; data from de Blok et al. 1995, 1996), normal face-on spirals (full dots; de Jong & van der Kruit 1994), and dwarf galaxies (crosses; Mellise & Israel 1994). LSB galaxies which are probably dwarf systems are indicated by triangles with crosses overlayed. Typical error bars are indicated in the bottom left of each panel.

galaxies along the Hubble sequence show a *continuous* range in central surface brightness, i.e. ranging from values around the Freeman value for early type systems to the very faint values observed for the late-type LSB galaxies in our sample (e.g. de Jong 1995; dB95).

LSB galaxies are usually much bluer, both in (B−V) and (R−I), and have fainter B magnitudes than their HSB counterparts (e.g. McGaugh 1992; vdH93; dB95). At a given gas mass, LSB galaxies are among the bluest disk galaxies observed (see below). Due to sample incompleteness, the distribution of galaxies in the (R−I) vs. B diagram (Fig. 6.1b) is limited to systems brighter than ~ -16 mag in the B band. Since photometric evolution models predict galaxies to evolve rapidly (i.e. within one Gyr) to colors (R−I)$\gtrsim +0.2$ mag (see Sect. 6.4), one expects to observe only a few galaxies with colors dominated by a young stellar population, i.e. with (R−I)$\lesssim +0.2$ mag. Three galaxies with (R−I)$\lesssim -0.1$ mag (i.e. F563-1 and two dwarfs) have been omitted from the data because their (R−I) colors are probably contaminated by nearby objects and/or suffer from large observational errors. Dwarf galaxies, on average, appear to be even bluer than LSB galaxies while spanning roughly the same range in luminosity.

The reason why LSB spirals are unusually blue compared to normal late type galaxies may be explained by the presence of a relatively young stellar population, the lack of internal dust extinction, and/or metallicity effects. Alternatively, the stellar mass function at birth in LSB galaxies may be different from that in HSB galaxies. We will discuss these possibilities in Sects. 6.4 and 6.5 below.

6.2.3 Abundances

Estimates of the ISM abundances in LSB galaxies predominantly rely on abundance determinations of their constituent HII regions. Within such regions, oxygen abundances are usually derived using an emperical relation for the line-ratio $R_{23} \equiv$ ([OII] $\lambda 3727$ + [OIII] $\lambda\lambda 4959, 5007$) / H$\beta$ as first discussed by Pagel et al. (1979) and later calibrated by e.g. McGaugh (1991). A full discussion of the method is given in McGaugh (1994) but we remark that for a given HII region observational errors in [O/H] can be as large as $\pm 0.2-0.3$ dex (apart from uncertainties due to internal reddening). For bright HII regions within the LSB galaxies listed in Table 6.1, abundances are taken both from McGaugh (1994) and de Blok & van der Hulst (unpublished).

We assume that the HII-region abundances on average are a reasonable indicator of the ISM abundances within a given LSB spiral. The intrinsic scatter in [O/H] among different HII region abundances within a given LSB galaxy is usually less than ± 0.2 dex around the mean HII region abundance (e.g. McGaugh 1994). However, in LSB galaxies containing only a few bright HII regions for which abundances have been determined, abundances may be biased towards the physical properties (e.g. age, initial metallicity and amount of self-enrichment) of individual HII regions (e.g. Pilyugin 1992; Pettini & Lipman 1995).

In Fig. 6.1c we compare mean [O/H] abundances of HII regions in LSB galaxies with those in HSB spirals (Zaritsky et al. 1994) and dwarf galaxies (Melisse & Israel 1994; Gallagher & Hunter 1986, 1987). On average, LSB galaxies seem to follow the correlation between the characteristic gas-phase abundance and luminosity as found for HSB spirals (Zaritsky et al. 1994). However, the range in [O/H] at a given B magnitude is nearly one dex and large scatter in the correlation is present. This scatter is probably related to evolutionary differences among the LSB galaxies of a given B magnitude (e.g. in the ratio of old to young stellar populations) and/or the HII regions they contain. Clearly, LSB galaxies (and dwarf systems) on average show substantially smaller [O/H] abundances than HSB galaxies.

As LSB galaxies have HI surface densities about a factor of $\sim$3 lower than in normal late-type galaxies (vdH93; dB96), their low [O/H] abundances may be interpreted in terms of a strong dependence of the SFR on surface density (see also Kennicutt 1989). Such a dependence has been suggested for late-type HSB galaxies (e.g. Edmunds & Pagel 1984; Dopita 1990; Phillips and Edmunds 1991; Ryder & Dopita 1994) and may apply to LSB galaxies as well (see Sect. 6.5).

6.2.4 Extinction

Estimates of extinction are particularly important when photometric evolution models are applied to spiral galaxies. Statistical studies of variations of galaxy magnitudes with inclination support the traditional view that Sc galaxies are semi-transparent with most of the extinction concentrated in the inner regions (e.g. Huizinga & van Albada 1992; Giovanelli et al. 1994). These studies conclude that the outer parts of spiral galaxies in general are optically thin.

Measurements of extinction in foreground spirals obscuring a background galaxy range from $\sim$0.3 mag in B in the interarm regions and outer parts of a spiral (Keel 1983; Andredakis & van der Kruit 1992; White & Keel 1992), to $\sim$1.6 mag within the spiral arms itself (Keel 1983; James & Puxley 1993). These studies suggest that internal extinction in HSB spirals is concentrated towards the galaxy nucleus and spiral arms, while extinction in the outer galaxy and inter-arm regions is relatively low. This is consistent with

conclusions derived from independent extinction studies for large samples of spiral galaxies (see also Jansen et al. 1994; Peletier et al. 1995; Huizinga 1995; Beckman et al. 1996).

Dust radiative transfer models indicate an overall face-on extinction in spirals of $\lesssim$0.5 mag in B (e.g. Knapen & van der Kruit 1991; Byun et al. 1994; Huizinga 1994), while estimates of the *maximum* face-on extinction in spirals based on far-IR measurements are in the range 1.5 to 2 mag in B (Disney et al. 1989). No support for optically thick disks has been found in a sample of nearby spirals from 60μm observations (Bothun & Rogers 1992). These studies support the idea that spiral galaxies have face-on extinctions of typically less than $\sim$0.5$-$1 mag in B.

The observational finding by Bosma et al. (1992) and Byun (1992) that low luminosity spirals appear transparent throughout their edge-on disks, while more luminous spirals become optically thick at a given galactocentric distance, supports the idea that face-on extinction in LSB galaxies is relatively low, i.e. typically less than $E_{B-V} = 0.1$ mag (e.g. McGaugh 1994). This is consistent with observational evidence in support of low dust contents in galaxies having low gas abundances (e.g. Issa et al. 1991; van den Hoek & de Jong 1992). In addition, low column densities of HI imply a low dust content if the gas-to-dust ratio is the same as (or larger than) in the Galaxy.

We consider $E_{B-V}\sim$ 0.5$-$0.6 mag as a plausible upper limit for the face-on extinction in spirals (assuming $R_V = A_V$ / $E_{B-V} \sim 3$ in our own Galaxy; e.g. Johnson 1968). In normal HSB spirals, we estimate typical face-on reddenings of $E_{B-V} \sim$ 0.3$-$0.4 and $\sim$ 0.1$-$0.2 mag, in systems with prominent and conspicuous spiral arms in their outer disk, respectively. In LSB spirals, which usually do not show either a strong nucleus or well developed spiral arms, face-on internal extinction is expected to be rather low, i.e. less than $E_{B-V} \sim 0.1$ mag.

6.2.5 Gas masses

We compare in Fig. 6.1d the present-day amounts of atomic gas $M_g \sim 1.4\ M_{HI}$ (corrected for helium) in LSB galaxies with those present in HSB galaxies and dwarfs. At a given B-band luminosity, LSB galaxies are usually found among the spirals containing the highest gas masses (dwarfs appear concentrated to somewhat smaller gas masses). Thus, since their HI surface densities are relatively low (dB96), LSB galaxies must have a larger, more extended disk of gas compared to that of HSB galaxies of the same luminosity (Zwaan et al. 1995).

The above strictly applies to the atomic gas content of galaxies only, since the inclusion of molecular gas may change the observed trend. If HSB spirals would be as gas-rich as LSB spirals of the same luminosity, HSB galaxies would need to contain at least $\sim$5 times more molecular gas than atomic hydrogen. This seems exceedingly high. For instance, our own Galaxy contains only as much H_2 as HI (Scoville & Sanders 1987). Furthermore, estimates of the amounts of molecular gas in normal Scd galaxies exclude H_2 / HI ratios larger than $\sim$ 1 (Young & Knezek 1989; Young & Scoville 1991).

So far no CO-emission has been detected in LSB galaxies (Schombert et al. 1990; de Blok & van der Hulst, in prep.). Therefore, the total amount of molecular gas in LSB galaxies is probably small even though relatively high CO/H_2 conversion factors may apply in these low metallicity galaxies (Wilson 1995). We will assume that the atomic hydrogen masses listed in Table 6.1 (multiplied by 1.4 to correct for He) represent the total amounts of gas in LSB galaxies. We conclude that, on average, LSB galaxies are considerably more gas-rich (up to a factor $\sim$ 3) than HSB galaxies *of the same luminosity* (see also Fig. 6.1g; and dB96). This implies that evolutionary differences between galaxies differing in surface brightness must exist (see Sect. 6.5).

6.2.6 Total masses and gas fractions

In principle, determination of the gas-to-total mass-ratio ($\mu_1 \equiv M_{gas}$ / ($M_{gas} + M_{stars}$)) of the matter contained within a given galactocentric radius (i.e. usually up to where the HI rotation curve can be measured), involves the conversion of the observed galaxy luminosity to stellar mass. However, the mass-to-light ratio of the underlying stellar population is generally not well known and, in fact, is an important quantity to determine. Alternatively, if one assumes a fixed value of the mass-to-light ratio, artificial trends will be introduced in the gas-fractions derived since this ratio is expected to vary among galaxies having different star formation histories. We note that, from theoretical point of view, μ_1 is strictly related to the amount of gas that is associated with the star forming disk and is available for star formation.

Independent estimates of the gas fraction μ_1 can be obtained from gas-to-dynamical mass-ratios $\mu_{dyn} \equiv M_{gas}/M_{dyn}$. However, since the dynamical masses of LSB galaxies usually include dark matter (i.e. matter not observed as gas or stars), values of μ_{dyn} provide lower limits to the actual gas fractions in LSB galaxies.

We determined $\mu_{\rm dyn}$ for a dynamical mass corresponding to the outermost point of the HI rotation curve (see dB96; Table 6.1).

For late-type HSB galaxies, studies by Bosma (1978), Begeman (1987), and Broeils (1992) have shown that the ratio of dark to luminous matter at the edge of the optical disk is $\sim 50\%$. In this case, the true gas fraction is underestimated by a factor ~ 2. The discrepancy probably increases for LSB galaxies and dwarfs (i.e. up to factors 2–10; see Broeils 1992), but is almost negligible in early-type HSB galaxies where the stellar population dominates the optical disk.

To get around the discrepancy for LSB galaxies, we also determined gas fractions $\mu_{\rm rot} \equiv M_{\rm gas} / (M_{\rm gas} + M_{*,\rm max})$ where $M_{*,\rm max}$ denotes the mass of the stellar component obtained from maximum disk fitting of the rotation curve (dB96). This method likely overestimates the contribution of the luminous stellar disk to the observed total mass distribution (e.g. Kuijken & Gilmore 1989; Bottema 1995) and, therefore, also provides a lower limit to the actual gas fraction.

In the following, we will use $\mu_{\rm rot}$ for LSB galaxies whenever the data allows application of the maximum disk method (cf. Table 6.1). We estimate that $\mu_{\rm rot}$ approximates the true gas fraction μ_1 within a factor of ~ 2. For LSB galaxies, we find that $\mu_{\rm rot}$ is 3–10 times larger than $\mu_{\rm dyn}$. This is consistent with the factors estimated by Broeils (1992) and suggests that LSB galaxies are dark matter dominated (see dB96).

For the HSB galaxies and dwarfs in our comparison samples, we are forced to use $\mu_{\rm dyn}$ as estimate of the actual gas fraction μ_1 as $\mu_{\rm rot}$ has been derived for a few of these systems only. Consequently, the adopted gas fractions are hard lower limits for all galaxies considered. We note that for HSB galaxies, the differences between $\mu_{\rm rot}$ and $\mu_{\rm dyn}$ are usually small (e.g. dB96).

Figs. 1e and 1f show the distribution of the present-day gas fraction $\mu_{\rm rot}$ and total gas mass vs. (B–V). It can be seen that LSB galaxies and dwarfs exhibit much larger gas fractions (typically $\mu_1 \sim 0.5$) than HSB spirals ($\mu_1 \sim 0.05$). This implies that LSB galaxies are in a low evolutionary state with respect to HSB spirals consistent with our earlier findings.

6.2.7 Mass-to-light ratios

We show in Figs. 1g and h the distribution of the mass-to-light ratio $M_{\rm HI}$ / L_B vs. (B–V) and vs. μ_1, respectively. LSB galaxies exhibit considerably higher $M_{\rm HI}$ / L_B ratios than HSB spirals (cf. Table 6.1). This is primarily due to the relatively large atomic gas contents of LSB spirals as discussed above. In addition, high values of $M_{\rm HI}$ / L_B may originate from a less well developed (both old and young) stellar population. In either case, the high values of $M_{\rm HI}$ / L_B observed for LSB spirals indicate a low evolutionary state of these galaxies. This is consistent with the fact that central surface brightnesses decrease with increasing values of $M_{\rm HI}$ / L_B as found for LSB galaxies (dB96).

We conclude that the low surface densities and brightnesses, blue colors, low abundances, large scale lengths, inconspicuous spiral arms and nuclei, low rotation velocities (dB96), and high gas masses observed in LSB spirals, all provide evidence in support of the view that LSB galaxies are relatively unevolved systems compared to HSB spirals. This agrees well with our finding that LSB galaxies usually display properties intermediate to those of HSB spirals and dwarf galaxies.

6.3 Model description and assumptions

We describe the galactic evolution model developed to study the chemical and spectro-photometric evolution of LSB galaxies (for a more extensive description of the model see van den Hoek 1997). We concentrate on the stellar contribution to the total galaxy luminosity in a given passband (other contributions are neglected). For a given star formation history (SFR), we compute the chemical enrichment of a model galaxy by successive generations of evolving stars. To derive the stellar luminosity in a given passband at a given age, we use an up-to-date metallicity dependent set of theoretical stellar isochrones as well as a library of spectro-photometric data. The spectro-photometric properties of the model galaxy are calculated by integrating the stellar luminosities at a given galactic age weighed by the SFR at the time these stars were born.

6.3.1 Chemical evolution model

We restrict ourselves to a brief outline of the basic assumptions and boundary conditions to the chemical evolution model used. We start from a model galaxy initially void of stars. We follow the chemical enrichment of this galaxy during its evolution assuming stars to be formed according to a given Pstar formation rate (SFR) and initial mass function (e.g. a power law IMF: $dN/dm \equiv M(m) \propto m^{\gamma}$). Specific choices of the SFR will be described in Sect. 6.4. Both stellar and interstellar abundances as a function of galactic evolution

time t are computed assuming that the stellar ejecta are returned and homogeneously mixed to the ISM at the end of their lifetimes (i.e. relaxing the instantaneous recycling approximation; see Searle & Sargent 1972). A description of the set of galactic chemical evolution equations used can be found in e.g. Tinsley (1980) and Twarog (1980), see also van den Hoek (1997).

We follow the stellar enrichment of the star forming galaxy in terms of the characteristic element contributions of Asymptotic Giant Branch (AGB) stars, SNII and SNIa. This treatment is justified by the specific abundance patterns observed within the ejecta of these stellar groups (see e.g. Trimble 1991; Russell & Dopita 1992). A detailed description of the metallicity dependent stellar lifetimes, element yields, and remnant masses is given by van den Hoek (1997) and van den Hoek & Groenewegen (1997). We compute the abundances of H, He, O, and Fe, as well as the heavy element integrated metal-abundance Z (for elements more massive than helium), during the evolution of the model galaxy. Both the SFR, IMF and resulting element abundances as a function of galactic evolution time, are used as input for the spectro-photometric evolution model described below.

Boundary conditions to the chemical evolution model are the galaxy total mass $M_{\rm tot}$, its evolution time $t_{\rm ev}$, and the initial gas abundances. Unless stated otherwise, we assume $M_{\rm tot} = 10^{10}$ $M_{\odot}$ and $t_{\rm ev} =$ 14 Gyr. For a given value of $M_{\rm tot}$, we normalise the model SFR such that a gas-to-total mass-ratio $\mu_{\rm l} \sim 0.1$ is reached at $t = t_{\rm ev}$. Note that solutions of the galactic chemical evolution equations are independent of the *ratio* of the SFR normalisation and $M_{\rm tot}$. Primordial helium and hydrogen abundances are adopted as $Y_{\rm p} = 0.232$ and $X = 0.768$ (cf. Pagel & Kazlauskas 1992). Initial abundances for elements heavier than helium are set to zero.

Table 6.2 IMF related parameters and stellar enrichment

γ	−2.35	slope of power-law IMF
$(m_{\rm l}, m_{\rm u})$	(0.1, 60) $M_{\odot}$	stellar mass range at birth
$(m_{\rm l}^{\rm AGB}, m_{\rm u}^{\rm AGB})$	(0.8, 8) $M_{\odot}$	progenitor mass range for AGB stars
$(m_{\rm l}^{\rm SNII}), m_{\rm u}^{\rm SNII})$	(8, 30) $M_{\odot}$	progenitor mass range for SNII
$(m_{\rm l}^{\rm SNIa}, m_{\rm u}^{\rm SNIa})$	(2.5, 8) $M_{\odot}$	progenitor mass range for SNIa
$\nu^{\rm SNIa}$	0.015	fraction of progenitors ending as SNIa

We list the main input parameters in Table 6.2, i.e. the adopted IMF-slope, minimum and maximum stellar mass limits at birth as well as the progenitor mass ranges for stars ending their lives as AGB star, SNIa, and SNII, respectively. For simplicity, we assume the stellar yields of SNIb,c to be similar to those of SNII. Furthermore, we assume a fraction $\nu^{\rm SNIa} = 0.015$ of all white dwarf progenitors with initial masses between $\sim$ 2.5 and 8 $M_{\odot}$ to end as SNIa. These and other particular choices for the enrichment by massive stars are based on similar models recently applied to the chemical evolution of the Galactic disk (e.g. Groenewegen, van den Hoek & de Jong 1995; van den Hoek & de Jong 1997). We will adopt these values also when modelling the stellar enrichment in LSB galaxies. We emphasize that the detailed inclusion of the stellar enrichment in LSB galaxies is important for their spectro-photometric evolution and is relevant for the qualitative conclusions presented below. Quantities used in the chemical evolution model are identical to those used in the spectro-photometric evolution part of the model.

6.3.2 Spectro-photometric evolution model

In principle, the total luminosity of a galaxy in a specific wavelength interval $\Delta\lambda$ is determined by: 1) the contribution by its stellar content L_*, 2) the contribution from the interaction between stars and gas $L_{\rm ism}$ (e.g. HII-regions, high-energy stellar outflow phenomena, etc.), and 3) the total amount of radiation absorbed $L_{\rm ext}$ (or scattered to wavelengths in- or outside $\Delta\lambda$) by gas and dust contained within the galaxy:

$$L_{\rm gal}^{\Delta\lambda}(t) = L_* + L_{\rm ism} - L_{\rm ext} \tag{6.1}$$

where each term in general is a complex function of galactic evolution time. We concentrate on the stellar contribution and neglect the latter two terms in Eq. (6.1). In this case, the galaxy luminosity within a waveband $\Delta\lambda$ at galactic evolution time t =T can be written as:

$$L_{\rm gal}^{\Delta\lambda}(t = {\rm T}) \; =$$

$$\int_{t=0}^{\rm T} \int_{m_{\rm l}}^{m_{\rm o}({\rm T}-t)} L_*^{\Delta\lambda}(m, Z(t), {\rm T}-t) \; S(t) M(m) \; {\rm d}m{\rm d}t \tag{6.2}$$

where m_l denotes the lower stellar mass limit at birth, $m_o(t)$ the turnoff mass for stars evolving to their remnant stage at evolution time t, and $L_*^{\Delta\lambda}$ the luminosity of a star with initial mass m, initial metallicity $Z(t)$, and age (T$-t$). We assume a separable SFR: $S(m,t) = S(t)M(m)$ where $S(t)$ is the star formation rate by number [yr^{-1}] and $M(m)$ the IMF [M$_\odot$ $^{-1}$]. By convention, we normalise the IMF as $\int M(m)\ dm = 1$ where the integration is over the entire stellar mass range $[m_l, m_u]$ at birth (cf. Table 6.2).

Starting from the chemical evolution model described above, we compute the star formation history $S(m,t)$, gas-to-total mass-ratio $\mu(t)$, and age-metallicity relations (AMR) $Z_i(t)$ for different elements i. Thus, at each galactic evolution time t the ages and metallicities of previously formed stellar generations are known. To derive the stellar passband luminosity $L_*^{\Delta\lambda}$ we use a set of theoretical stellar isochrones, as well as a library of spectro-photometric data. Stellar evolution tracks provide the stellar bolometric luminosity $L_*^{\rm bol}$, effective temperature $T_{\rm eff}$, and gravity g, as a function of stellar age for stars with initial mass m born with metallicity Z_*. We compute Eq. (6.2) using a spectro-photometric library containing the stellar passband luminosities $L_*^{\Delta\lambda}$ tabulated as a function of $T_{\rm eff}$, Log g, and Z_* (see below).

We emphasize that the turnoff mass m_o(T $- t$) occuring in Eq. (6.2) depends on the metallicity $Z(t)$ of stars formed at galactic evolution time t. For instance, the turnoff mass for stars born with metallicity $Z = 10^{-3}$ at a galactic age of $t_{\rm ev} = 14$ Gyr is $m_o \sim 0.8$ M$_\odot$ (e.g. Schaller et al. 1992). This value differs considerably from $m_o \sim 0.95$ M$_\odot$ for stars born with metallicity Z= Z$_\odot$. Such differences in m_o affect the detailed spectro-photometric evolution of a galaxy by constraining the mass-range of stars in a given evolutionary phase (e.g. horizontal branch) at a given galactic evolution time. In the models described below, we explicitly take into account the dependence of $m_o(t)$ on the initial stellar metallicity Z_* (see van den Hoek 1997).

6.3.3 Stellar evolution tracks and spectro-photometric data

We use the theoretical stellar evolution tracks from the Geneva group (e.g. Schaller et al. 1992; Schaerer et al. 1993). These uniform grids are based on up-to-date physical input (e.g. opacities, nuclear reaction rates, mixing schemes, etc.) and cover large ranges in initial stellar mass and metallicity, i.e. $m = 0.05 - 120$ M$_\odot$ and Z= 0.04 $-$ 0.001, respectively. These tracks imply a revised solar metallicity of $Z_\odot = 0.0188$ with $Y_\odot = 0.299$, and $\Delta Y/\Delta Z = 3.0$ for a primordial He-abundance of $Y_{\rm p} = 0.232$. For stars with $m >$ 7 M$_\odot$, these tracks were computed until the end of central C-burning, for stars with $m = 2-5$ M$_\odot$ up to the early-AGB, and for $m < 1.7$ M$_\odot$ up to the He-flash. For stars with $m \lesssim 0.8$ M$_\odot$, we used the stellar isochrone program from the Geneva group (Maeder & Meynet, private communication).

To cover the latest stellar evolutionary phases (i.e. horizontal branch (HB), early-AGB, and AGB) for stars with $m \lesssim 8$ M$_\odot$, we extended the tracks from Schaller et al. with those from Lattanzio (1991; HB and early-AGB) for $m \sim 1 - 2$ M$_\odot$, and from Groenewegen & de Jong (1993; early-AGB and AGB) for $m \sim 1 - 8$ M$_\odot$. These tracks roughly cover the same metallicity range as the tracks from the Geneva group. The synthetic AGB models from Groenewegen & de Jong were succesfully applied to AGB stars both in the Galactic disk and Magellanic Clouds (see also Groenewegen, van den Hoek & de Jong 1995). Special attention has been paid to smoothly fit together these distinct data sets. Corresponding isochrones were computed at a carefully selected logarithmic grid of stellar ages, well covering galactic evolution times up to $t_{\rm ev} \sim 14$ Gyr. Isochrones are linearly interpolated in m, log Z, and log t.

The spectro-photometric data library that we use is based on the Revised Yale Isochrones and has been described extensively by Green et al. (1987). These data include stellar UBVRI Johnson-Cousins magnitudes covering the following ranges in $T_{\rm eff}$[K] = 2800 to 20000, log g [cm s^{-2}] = -0.5 to 6, and log $(Z/Z_\odot) \sim -2.5$ to $+0.5$. Corresponding spectro-photometric data for stars with $T_{\rm eff} > 20000$ K have been adopted from Kurucz (1979) at solar metallicity, covering $T_{\rm eff} = 20000 - 50000$ K.

6.4 Model tuning, uncertainties, and selection

6.4.1 Model calibration

For the photometric evolution model discussed in the previous section, we show in Fig. 6.2 the evolution of the (U$-$B), (B$-$V), (V$-$R), (V$-$I) colors, and the stellar mass-to-light ratio M$_*$ / L$_{\rm tot}$, of a single stellar population formed at $t = 0$ with initial stellar metallicities $Z = 0.02$, 0.008, and 0.001, respectively. We note that our models are dust-free and have been computed at a time resolution of log $(\Delta t$[yr]) $\sim$6).

We compare the model adopted in this paper with the recent photometric evolution models presented by Worthey (1994) and Bressan et al. (1994). In brief, the model of Worthey includes the metallicity dependent stellar evolution tracks of van den Berg (e.g. 1985) up to the base of the red giant branch (RGB), the Revised Yale Isochrones (Green et al. 1987) up to the tip of the RGB, and post RGB tracks from

different literature sources. The model of Bressan et al. comprises a homogeneous library of metallicity dependent stellar evolution tracks up to the end of the early AGB (or the onset of central carbon ignition) presented by Alongi et al. (1993) and Bressan et al. (1994). Both models use the stellar spectral flux library from Kurucz (1992) and determine colors and magnitudes by convolution of the integrated spectral energy distribution of a stellar population with the UBVRI pass-band filters.

Comparison of the UBV colors predicted by the model used in this paper with those given Worthey (1994) and Bressan et al. (1994) reveals that these models provide very similar results. Note that the selected colors in general become bluer with decreasing initial metallicity (metallicity effects in the R and I band are usually small; see also Worthey 1994). Particularly good overall agreement is found between the photometric results of Worthey and that developed by us (even though distinct libraries of stellar isochrones were used).

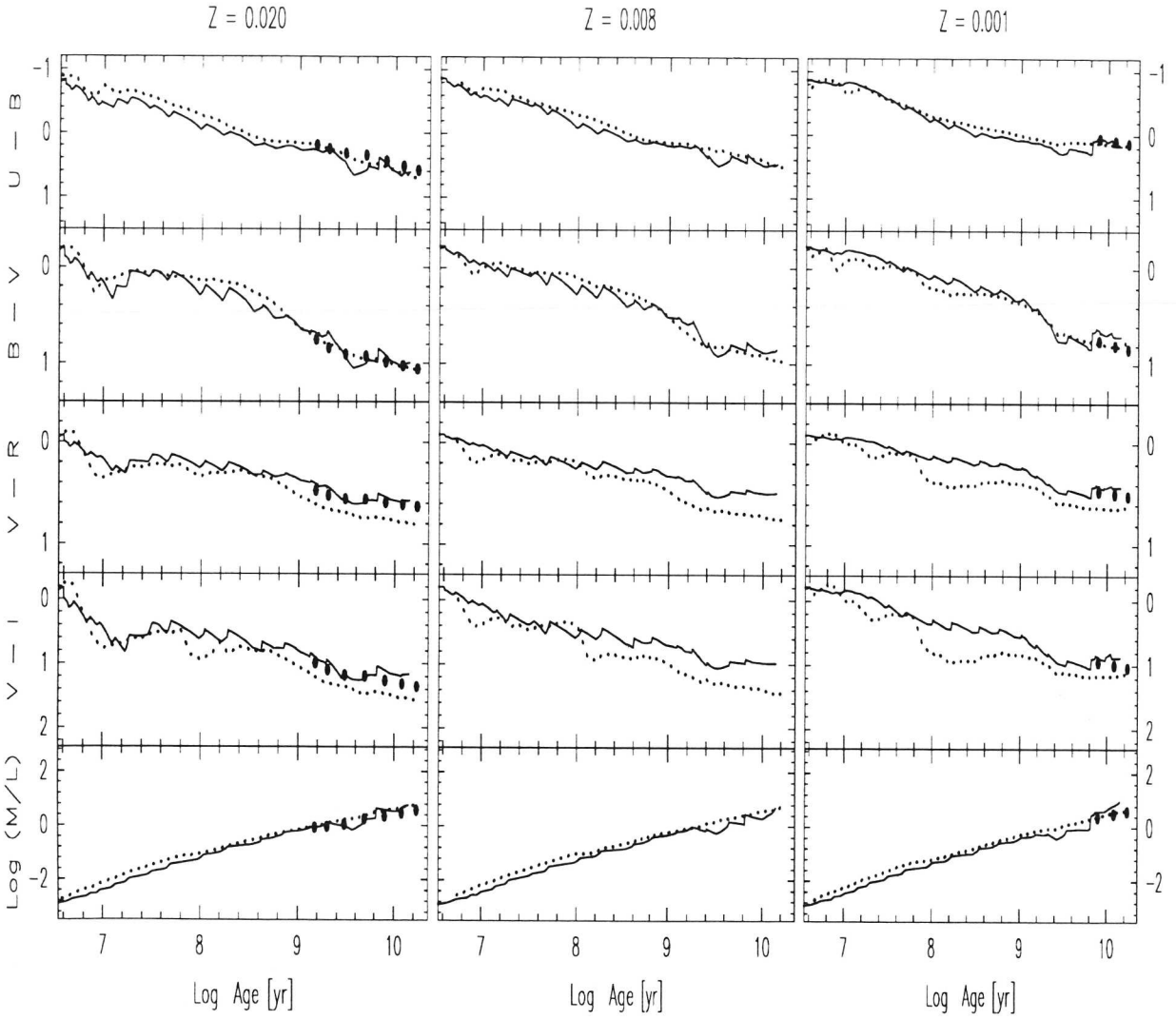

Figure 6.2 Theoretical UBVRI colors and stellar mass-to-light ratio evolution of a single stellar population with initial metallicity Z =0.02 (left panels), Z = 0.008 (center), and Z = 0.001 (right panels). Photometric evolution models refer to: Worthey (1994, full circles), Bressan et al. (1994, dashed lines), this paper (solid curves)

In general, the Bressan et al. model predicts R and I band magnitudes that are somewhat brighter ($\sim 0.1-0.4$ mag) at ages $\gtrsim 1$ Gyr at $Z = 0.02$ (and at ages $\gtrsim 0.1$ Gyr at $Z \lesssim 0.008$) than predicted by the other models. This is due to the fact that Bressan et al. used the Johnson RI filter passbands (as supplied with the Kurucz 1992 distribution) which are known to result in ($V-R_J$) and ($V-I_J$) colors that are too red for cool stars (see e.g. Worthey 1994). The stellar mass-to-total light ratios vs. log Age predicted by the different models are in good agreement. Variations in M/L_{tot} with metallicity are found negligble. In contrast, mass-to-light ratios for different passbands show a strong metallicity dependence, which reverses when going from blue to near-IR colors (Worthey 1994).

Although a detailed description of the tuning and calibration of the adopted photometric model is beyond the scope of this paper, we note that the model has been checked against various observations including integrated colors and magnitudes, luminosity functions, and color-magnitude diagrams of Galactic (and Magellanic Cloud) open and globular clusters covering a wide range in age and metallicity.

As an example, we show in Fig. 6.3 resulting color-magnitude diagrams for a Monte-Carlo simulation of the Galactic disk open cluster M67. We used the stellar photometry data (mainly from the Geneva group) described in Sect. 3.3. For M67, we assumed an age of 3.5 Gyr and metallicity $Z = 0.016$. These values are consistent with observations which suggest that M67 is a solar metallicity cluster with an age of ~4 Gyr (see Montgomery et al. 1993). Furthermore, a binary fraction of ~75% (see Sect. 3.3.6) was assumed (for binaries with mass-ratios $m_2/m_1 \lesssim 1$) and we adopted an extinction in the direction of M67 of E(B−V) = 0.05 mag as indicated by the observations.

Fig. 6.4 shows the corresponding color-magnitude diagrams observed for M67 presented by Montgomery et al. (1993). Very good agreement is found between the predicted and observed color-magnitude diagrams of M67 cluster stars. In particular, the precise location and shape of the main-sequence turnoff points as well as the locations of the red giant branches are well reproduced by the models. Note that the detailed positions of the cluster stars in the color-magnitude diagrams can be compared (i.e. not the relative number of stars of a given V magnitude since the model stars were not weighed by the IMF). Similar calibration tests were performed succesfully for open and globular clusters covering a wide range in age and metallicity. In general, good agreement was found between the predicted and observed color-magnitude diagrams of the clusters studied. We note that analogue comparisons have been presented e.g. by Worthey (1994) and Bressan et al. (1994).

6.4.2 Uncertainties and limitations

Although the previous comparison demonstrates that the adopted stellar evolution data are essentially correct and reliable, several uncertainties and sources of errors are involved in the photometric evolution model. These are related to the detailed assumptions and interpolations made in the evolutionary tracks used (e.g. amount of overshooting, mixing lengths, convection, nuclear reaction rates, etc.), and to the calibration of the stellar fluxes, magnitudes, and colors in the spectral library (e.g. temperature, gravity, chemical composition). Both the adopted stellar evolution tracks and stellar spectro-photometric library (accuracy and input physics, grid-range and interspacing, included stellar evolutionary phases, spectral range) determine to a large extent the final galaxy magnitude and color evolution. In addition, errors may arise because of differences in the filter transmission curves used to calculate synthetic magnitudes and those used with observations of e.g. galaxies (e.g. Bessell 1979).

Apart from these sources of errors, which are inherent to any photometric model used to predict the spectral evolution of a galaxy according to a given star formation history and chemical evolution, there are several uncertainties involved with the importance of binary stars, extinction, the detailed stellar mass function at birth and lower mass cutoff, initial element abundances (e.g. helium, oxygen) at a given metallicity, and the inclusion of late stages of stellar evolution which are relatively uncertain (e.g. post AGB and Wolf-Rayet stages). Although a detailed discussion of the above uncertainties is beyond the scope of this paper (see e.g. Worthey 1994; van den Hoek 1997), we do not expect these to alter the qualitative conclusions presented below. Overall, the models above are in good agreement with many independent aspects of stellar evolution theory which provides confidence for their application to more complex systems such as galaxies.

Nevertheless, the influence of binaries and the adopted IMF on the photometric evolution results may be relevant for the photometric evolution of LSB galaxies compared to that of HSB galaxies. Therefore, we will briefly address these effects when discussing model results below.

6.4.3 Model selection and properties

We present results for the chemical and spectro-photometric evolution model discussed in the previous section. We start from a model LSB galaxy with initial mass $M_g(t = 0) = 10^{10}$ $M_\odot$, initially metal-free and void of stars. The chemical and photometric evolution of this galaxy are followed during evolution time t_{ev} = 14 Gyr, assuming one of the theoretical star formation histories discussed below. Unless stated otherwise, we assume that stars are formed according to a Salpeter (1955) IMF (i.e. $\gamma = -2.35$) with stellar mass limits at birth between 0.1 and 60 $M_\odot$ (cf. Table 6.2).

A basic set of star formation histories is used to see how these models behave with respect to the observed properties of LSB spirals discussed in Sect. 6.2. The following functions of the SFR with galactic age are considered: 1) constant, 2) exponentially decreasing, 3) linearly decreasing, 4) exponentially increasing, and 5) linearly increasing. Normalized SFRs and resulting age-metallicity relations are shown in Fig. 6.5.

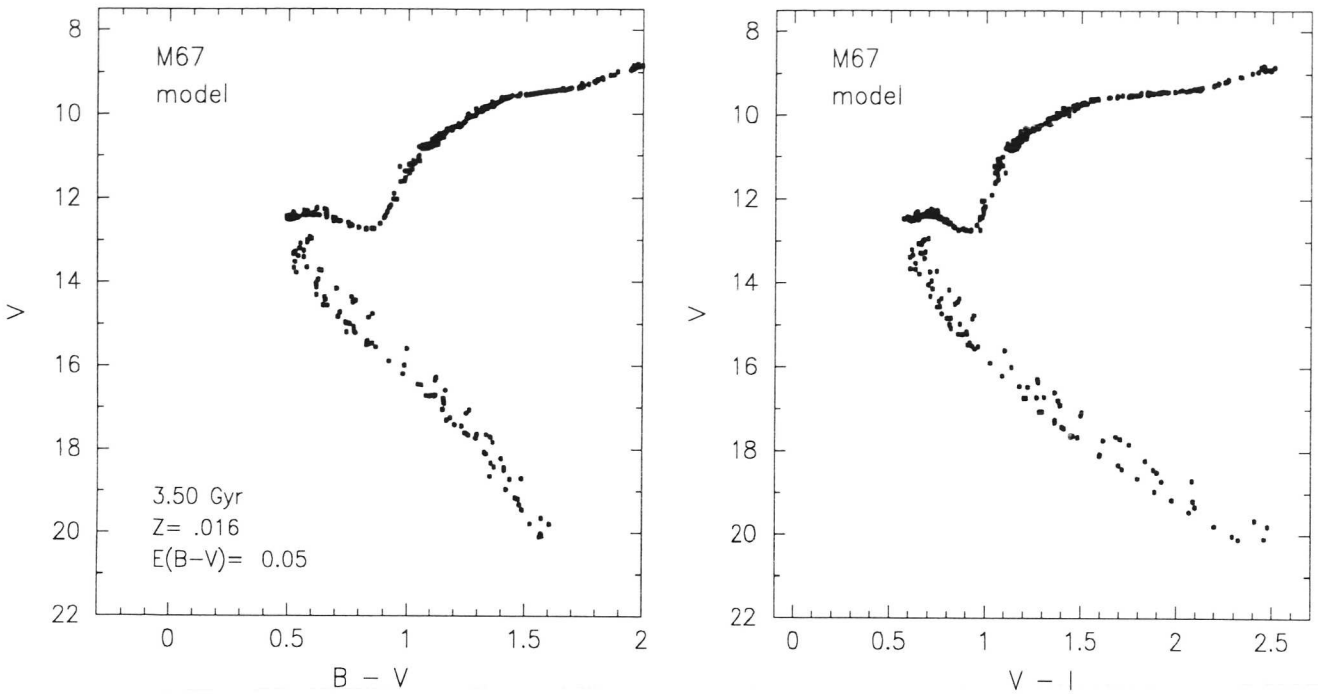

Figure 6.3 Monte-Carlo simulation of the Galactic disk open cluster M67. Resulting V vs. (B−V) and V vs. (V−I) distributions are shown for a single stellar population born with $Z = 0.016$ and age 3.5 Gyr. An extinction of E(B−V) = 0.05 mag and a binary fraction of 75% were assumed. Stars were selected randomly in mass but with absolute visual magnitudes $V \lesssim 20$ mag.

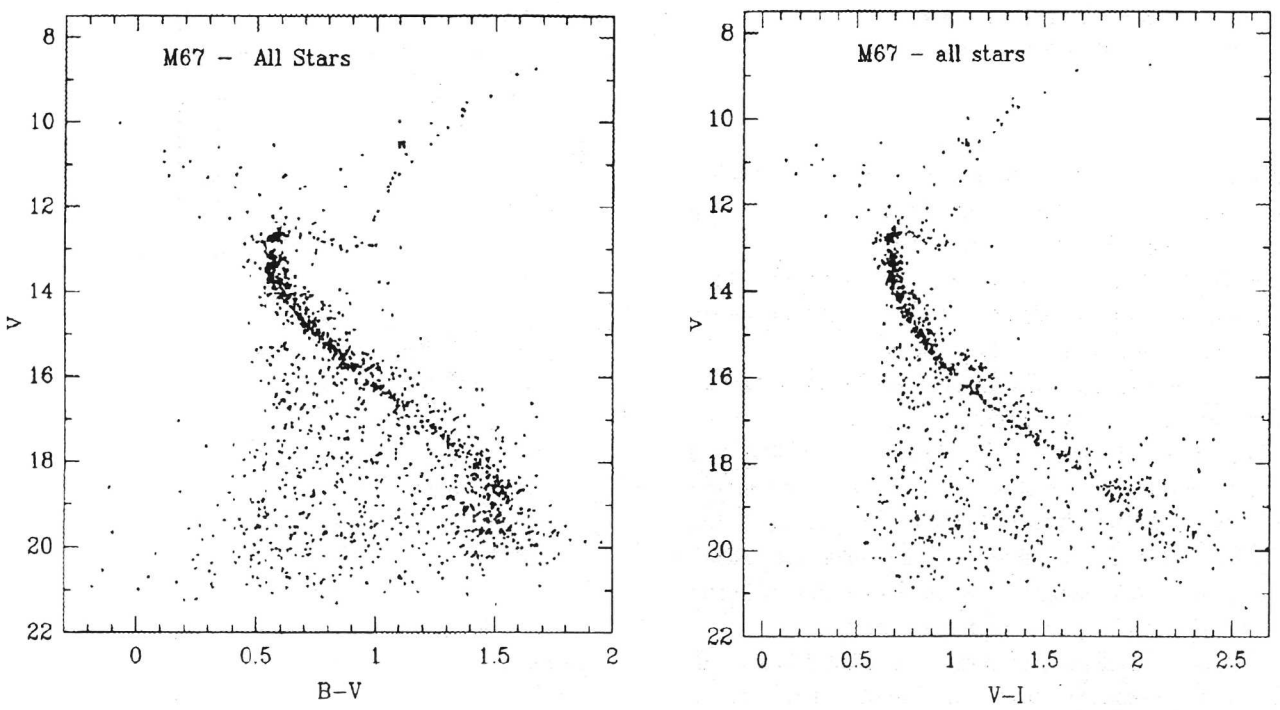

Figure 6.4 Observed V vs. (B−V) and V vs. (V−I) color-magnitude diagrams for all stars in the field of the open cluster M67 from Montgomery et al. (1993). Note that the main sequence is still visible down to the limit of the photometry (i.e. $V \sim 20$ mag). The binary sequence at ~0.7 mag above the main sequence can be distinguished. Stars below the main-sequence are presumably field stars.

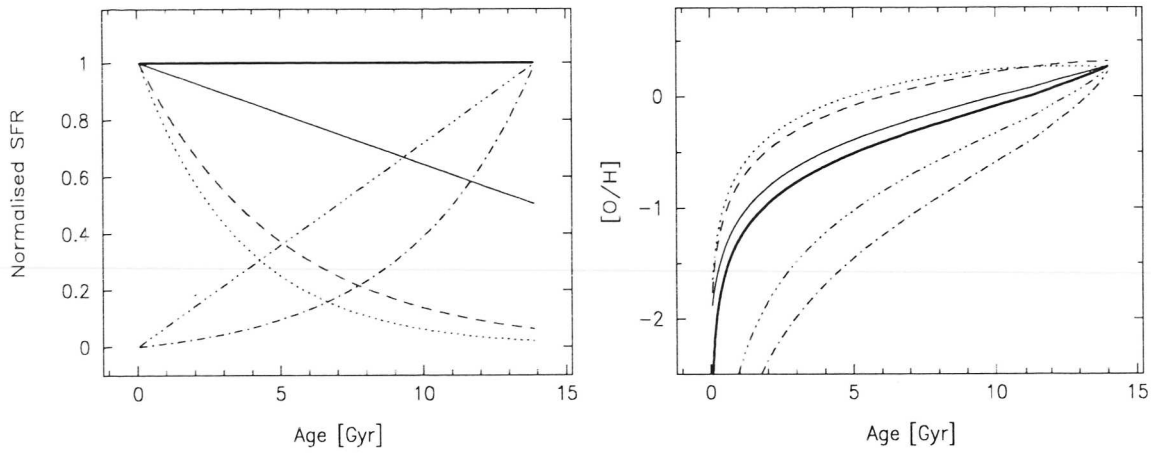

Figure 6.5 Basic set of star formation histories considered (**left**) and resulting [O/H] vs. age relations (**right**): constant SFR model (thick solid line), linearly decreasing (thin solid), exponentially decreasing (dashed; t_{sfr} = 5 Gyr), rapid exponentially decreasing (dotted; t_{sfr} = 4 Gyr), linearly increasing (dash-dotted), and exponentially increasing (dot-dashed). SFRs have been normalised to a current gas-to-total mass-ratio $\mu_1 = 0.1$.

Table 6.3 Basic set of star formation models ($\mu_1 = 0.1$ and $M_{tot} = 10^{10}$ $M_\odot$, unless noted otherwise)

(1)	(2) Model	(3) <SFR> [$M_\odot$ yr^{-1}]	(4) SFR_1	(5) α	(6) $[O/H]_1$	(7) N_{tot}	(8) L_B [$L_{\odot,B}$]	(9) M_{HI} / L_B [$M_\odot L^{-1}_{\odot,B}$]	(10) IMF/SFR
A1	Exp. decreasing	0.93	0.17	0.18	+0.3	3.6(10)	3.6(9)	0.16	$\gamma = -2.35$, (+)
A2	"	0.52	0.09	0.18	−0.25	2.1(10)	2.3(9)	1.56	$\gamma = -2.35$,(+, I)
A3	"	0.69	0.13	0.18	−0.9	4.7(10)	1.6(9)	0.45	$\gamma = -3$, (+)
A4	"	1.08	0.20	0.18	+0.5	2.2(10)	5.2(9)	0.16	IMF: *, (+)
B1	Constant	0.89	0.89	1.	+0.3	3.4(10)	1.0(10)	0.03	$\gamma = -2.35$
B2	"	0.49	0.49	1.	−0.25	2.1(10)	6.4(9)	0.58	$\gamma = -2.35$, (I)
B3	"	0.68	0.68	1.	−0.9	4.7(10)	3.7(9)	0.21	$\gamma = -3$
B4	"	1.08	1.08	1.	+0.5	2.2(10)	1.7(10)	0.04	IMF: *
C	Exp. decreasing	0.90	0.07	0.08	+0.3	1.1(11)	2.3(9)	0.32	$\gamma = -2.35$, (x)
D	Lin. decreasing	0.90	0.60	0.67	+0.3	3.5(10)	7.6(9)	0.10	$\gamma = -2.35$
E	Exp. increasing	0.85	3.06	3.4	+0.3	3.3(10)	2.8(10)	0.03	$\gamma = -2.35$
F	Lin. increasing	0.87	1.74	2.0	+0.3	3.3(10)	1.8(10)	0.04	$\gamma = -2.35$

* Kroupa et al. IMF (1992) assumed; (+) τ_{sfr} = 5 Gyr; (x) τ_{sfr} = 4 Gyr; (I) $\mu_1 = 0.5$

For each model, the amplitude of the SFR is chosen such that a present-day gas-to-total mass-ratio μ_1 = 0.1 is achieved (indices 1 and 0 will be used to refer to current and initial values, respectively).

In columns (2) to (6) of Table 6.3, we list the functional form of the SFR, average past and current SFRs, the ratio of current and average past SFRs α, and the present-day oxygen abundance by mass. It can be verified that the average past SFR, $\langle SFR \rangle = 0.9$ $M_\odot$ yr^{-1}, is roughly the same for all models ending at $\mu_1 = 0.1$, assuming a Salpeter IMF and $M_g(t = 0) = 10^{10}$ $M_\odot$. In contrast, *present-day* SFRs range from $SFR_1 = 0.07$ to 3 $M_\odot$ yr^{-1} and in fact determine the contribution by young stars to the integrated light of the model galaxy (see below). Current oxygen abundances predicted are $[O/H]_1 \sim +0.25$ and are mainly determined by μ_1, the IMF, and the assumed mass limits for SNII (cf. Table 6.3).

Before comparing different SFR models with available observational data on LSB galaxies, we consider the photometric evolution of the constant and exponentially decreasing SFR models in some more detail. Fig 6.6 shows the evolution of the total number of MS and post-MS stars for the exponentially decreasing SFR model. The current total number of MS stars is roughly 4 10^{10}, compared to $\sim 10^8$ post-MS stars (all phases) and $\sim$ 3 10^4 (AGB stars only). Mean stellar luminosities for stars in distinct evolutionary phases decreased over the past 10−12 Gyr by about one order of magnitude for MS, RGB, and HB stars while remaining relatively constant for early-AGB (EAGB) and AGB stars. The present-day mean luminosity of stars on the MS is $\sim 10^{-1}$ $L_\odot$ compared to $\sim 10^4$ $L_\odot$ for AGB stars. Summing over all phases, the product

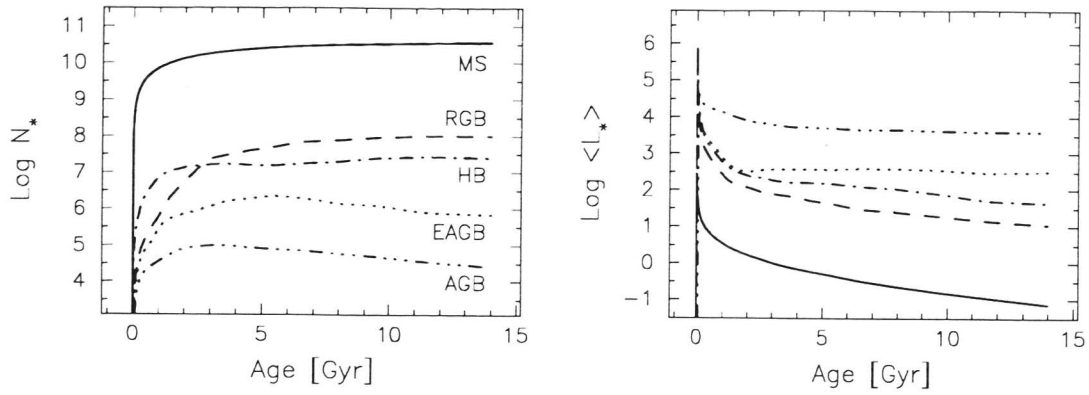

Figure 6.6 Exponentially decreasing SFR model: total number of stars formed (*left*) and average stellar bolometric luminosity (*right*) vs. galactic age for distinct evolutionary phases: MS (solid curve), RGB (dashed), HB (dot-dashed), EAGB (dotted), and AGB (dash-dotted).

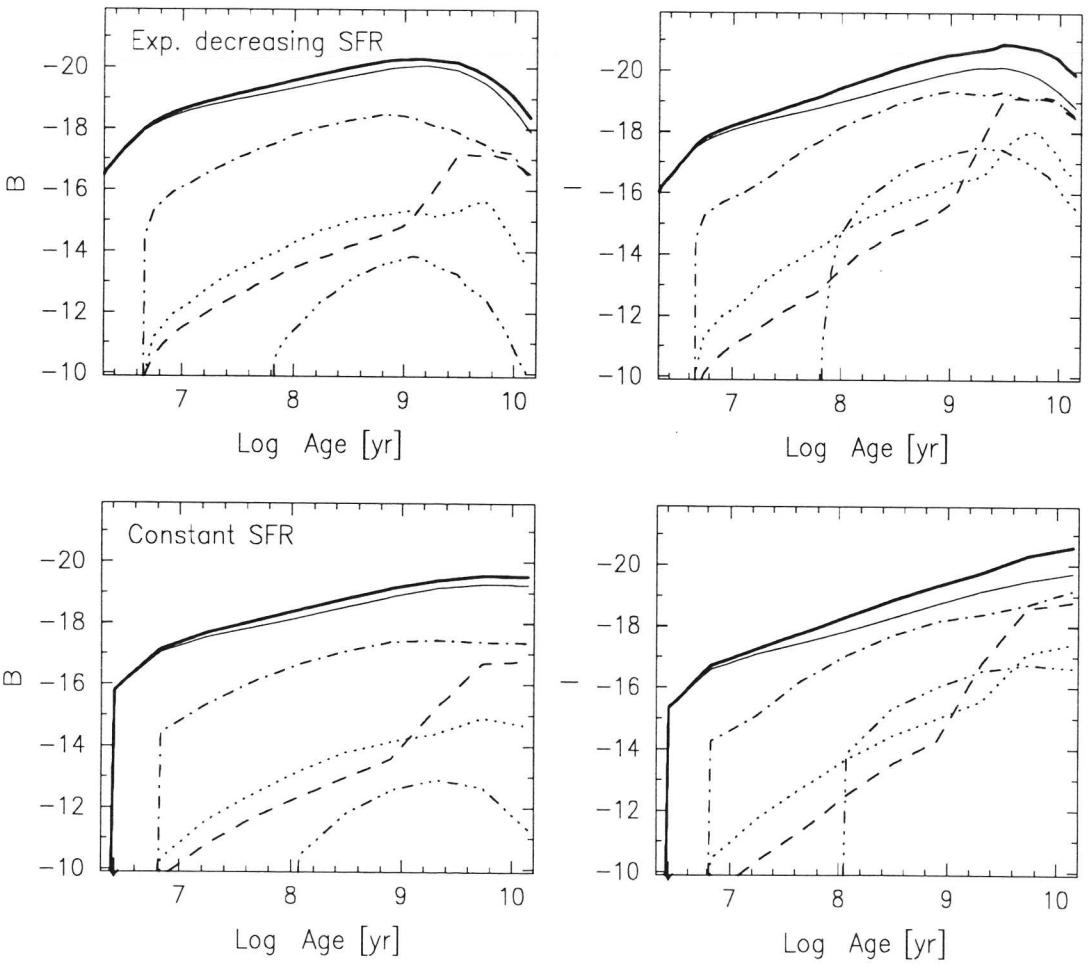

Figure 6.7 Photometric evolution of exponentially decreasing SFR (*top panels*) and constant SFR (*bottom*) models. *Left panels:* B-mag contribution for stars in distinct evolutionary phases as in Fig. 6.6: MS (solid curve), RGB (dashed), HB (dot-dashed), EAGB (dotted), AGB (dash-dotted), and Total (thick solid). *Right panels:* Same as left panels but for I-mag

of total number of stars and mean stellar luminosity, shows that the current bolometric galaxy luminosity is determined mainly by MS stars ($L_{MS} \sim 4\ 10^9\ L_\odot$). In particular, AGB stars ($L_{AGB} \sim 10^8\ L_\odot$) are relatively unimportant. This is characteristic of the constant and exponentially decreasing SFR models discussed here.

For the exponentially decreasing star formation model discussed in Fig. 6.6, we show in Fig. 6.7 the B and I-band magnitudes of stars in distinct evolutionary phases. As for the total galaxy luminosity, MS stars generally dominate in the B-band. However, within the I-band, RGB and HB stars are nearly as important as MS stars, at least at late stages of galactic evolution. Due to the cooling of old, low-mass MS stars as well as the contribution by RGB and HB stars increasing with galactic age, the current total I-band magnitude is considerably brighter than that in the B-band. We emphasize that this qualitative model behaviour is insensitive to the adopted star formation history (for *e-folding times larger than 3–5 Gyr) but instead is determined by the assumed IMF and the stellar input data used* (e.g. lifetime in each evolutionary phase, stellar evolution tracks, etc). Thus, constant star formation models exhibit a similar behaviour apart from being brighter by about one magnitude in all passbands at later evolution times (cf. Fig. 6.7).

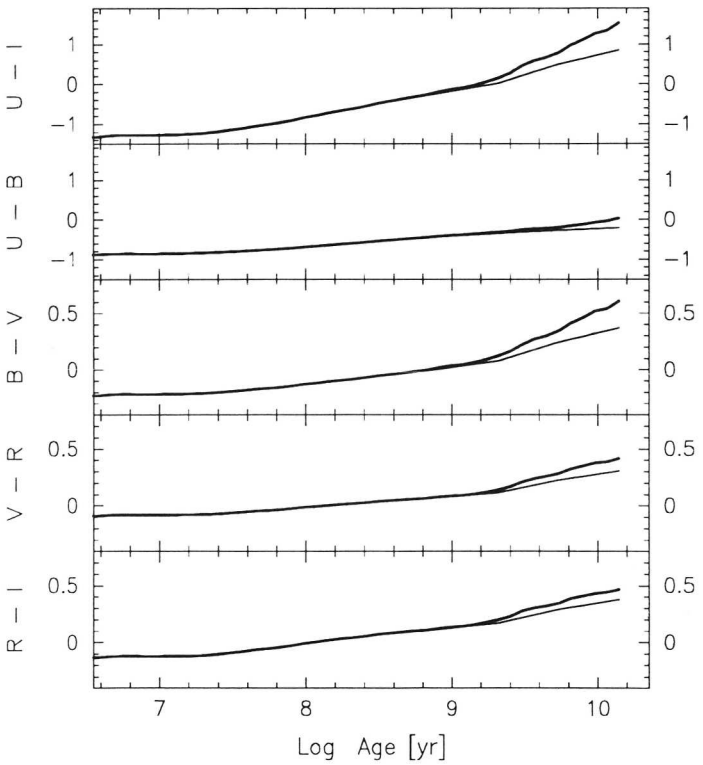

Figure 6.8 Broadband colours vs. galactic age for exponentially decreasing SFR (thick solid) and constant SFR (solid) models. Note the different magnitude scales in the upper two and bottom three panels, respectively.

Fig. 6.8 illustrates the sensitivity of broadband colors to the galactic star formation history for constant and exponentially decreasing SFR models. It can be seen that the colors considered increase with galactic age (most rapidly in U–I). In general, differences between colors such as (U–B), (B–V), and (R–I) for distinct SFR models are less than the variations of these colors with age for a given model, the largest differences occuring in (U–I) and (B–V). Also, assuming a galactic age since the onset of star formation of e.g. 8 instead of 14 Gyr has limited effect on the resulting galaxy colors (e.g. less than 0.1 mag in B–V), even though absolute magnitudes are substantially altered (cf. Fig. 6.7). We like to emphasize that both age and extinction effects can result in substantial reddening of the colors of a stellar population in almost the same manner and it is difficult to disentangle their effects on the basis of photometry data alone. Clearly, galaxy colors *alone* are not well suited to discriminate between distinct SFR models, even when internal extinction is low and other reddening effects are negligble (see below).

Fig. 6.9 demonstrates that the contribution by post-MS stars to the mean colors of a stellar population is usually limited to a few tenths of a magnitude. Therefore, the use of (B–V) and (R–I) colors as mean age indicator of the dominant stellar population is valid for the dust-free models discussed here (cf. Fig. 6.8). In particular, the mean age of an unreddened stellar population increases with (R–I), provided that AGB stars are negligible contributors to this color. Note that the detailed (R–I) vs. age relation given in Figs. 6.8 and 6.9 depends on the assumed IMF, SFR, and stellar evolution data used.

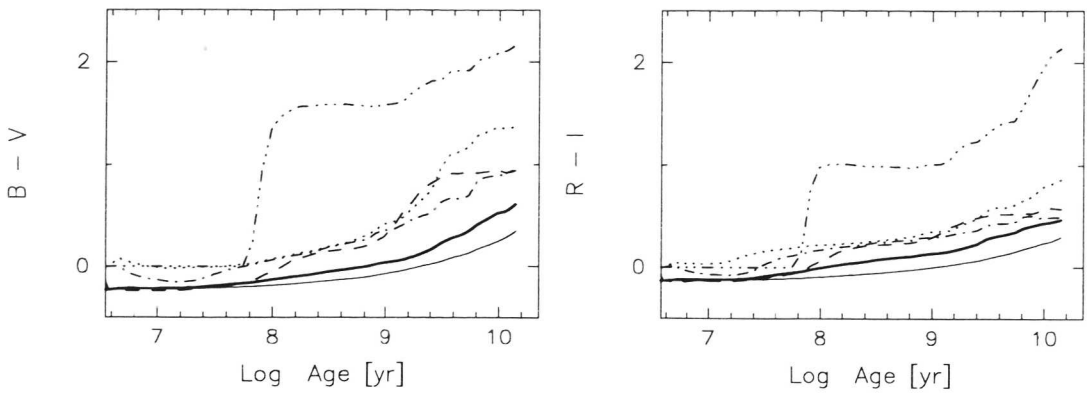

Figure 6.9 Exponentially decreasing SFR models: broadband (B−V) and (R−I) colors vs. galactic age. Mean colors for stars in distinct evolutionary phases as in Fig. 6.6: MS (solid curve), RGB (dashed), HB (dot-dashed), EAGB (dotted), AGB (dash-dotted), and Total (thick solid).

6.4.4 More detailed predictions

Fig. 6.10 illustrates in detail the properties (i.e. the luminosities, colors, effective temperatures, abundances, and masses) of the present-day stellar population predicted by the exponentially decreasing SFR model ($\tau_{\rm sfr}$ = 5 Gyr) ending at $\mu_1 = 0.1$. Results are shown for stars in different evolutionary phases from the main-sequence up to the AGB by means of a Monte-Carlo simulation. This figure serves to illustrate the main characteristics of the present-day stellar populations (with ages 14 Gyr) predicted by our models and can be compared both with observations and other spectro-photometric evolution models. Very similar results are obtained e.g. for exponentially decreasing SFR models ending at $\mu_1 = 0.5$ or constant SFR models.

Fig. 6.11 shows the corresponding luminosity, color, mass, and metallicity distributions for the present-day main-sequence stellar population shown in Fig. 6.10. Again, these distributions (such as the mass and luminosity function of main-sequence stars) can be compared directly to observations whenever such data is available. We emphasize that these distributions do not depend strongly on the adopted star formation history since the distributions are normalised to all stars (ever formed in the model galaxy) that are nowadays on the main-sequence. In contrast, these distributions are very sensitive to the stellar IMF at birth and, in principle, can be used to constrain the IMF.

In Fig. 6.12 we show the resulting present-day luminosity and number contributions of stars in different evolutionary phases as function of their age (corresponding to the results discussed in Figs. 6.11 and 6.10). For instance, Fig. 6.12 demonstrates that main-sequence stars younger than ~1 Gyr contribute nearly 75% to the total present-day U band luminosity of all main-sequence stars. Similarly, the contribution of main-sequence stars younger than 1 Gyr to the I band is less than ~25%. These results can be used to estimate the contribution of young stars to the present-day galaxy luminosity in a given wave band which, in principle, also can be determined observationally. Such observations provide valuable constraints to the underlying star formation history and stellar IMF at birth of the present-day stellar populations in galaxies. For comparison, Fig. 6.13 illustrates the same results for the constant SFR model ending at $\mu_1 = 0.1$ (see Fig. 6.5) and reveals the sensitivity of the present-day luminosity distributions of stars in different evolutionary phases to the underlying star formation history.

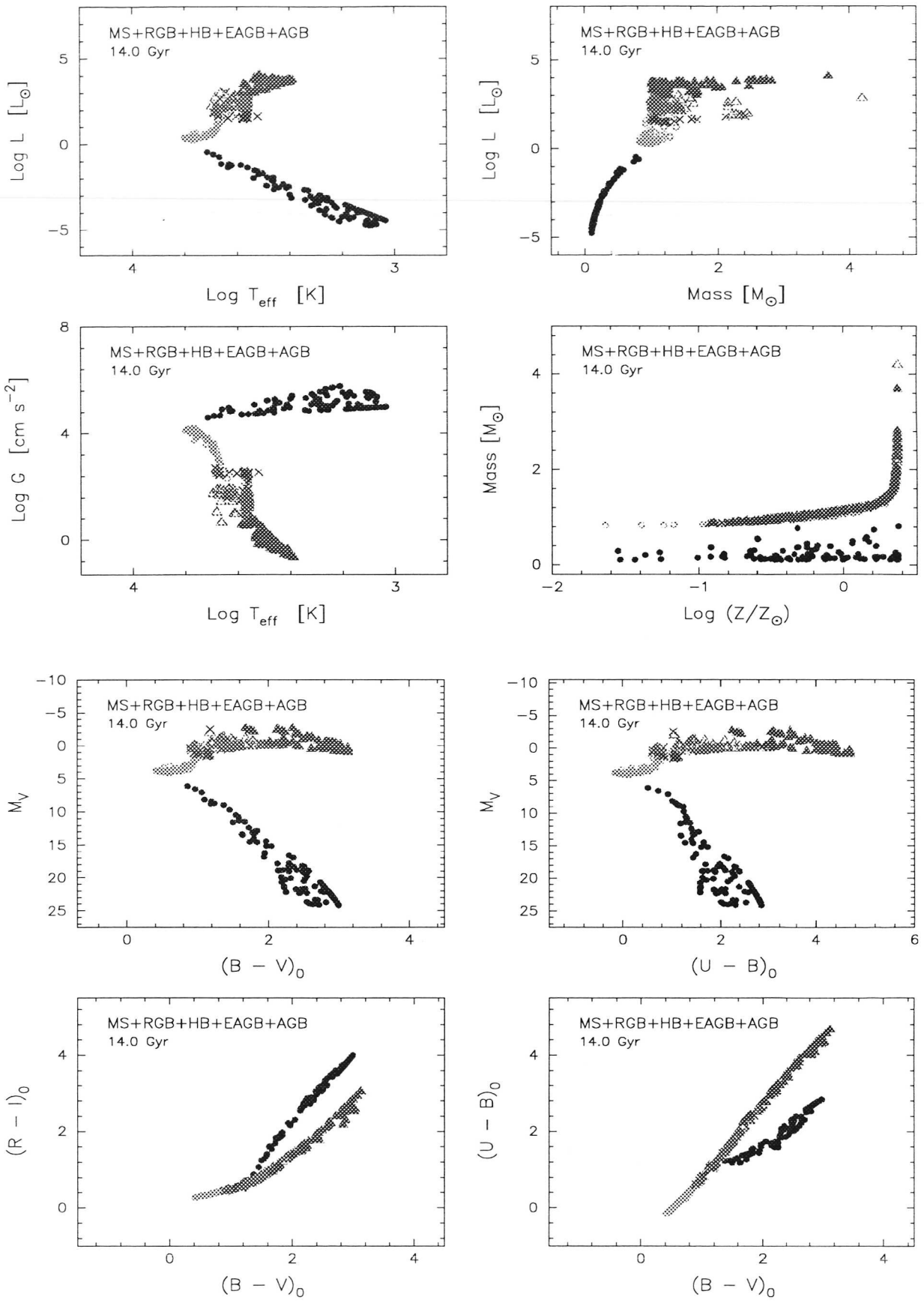

Figure 6.10 Predicted properties of individual stars in different evolutionary phases at galactic age t_{ev} =14 Gyr in case of the exponentially decreasing SFR model (τ_{sfr} = 5 Gyr) ending at μ_1 = 0.1. Stars were selected according to their present-day evolutionary phase (i.e. no IMF or SFR weighing was applied). For each phase, the properties of ~100 stars were plotted as follows: MS (*full circles*), RGB (*open circles*), HB (*crosses*), EAGB (*open triangles*), and AGB (*full triangles*).

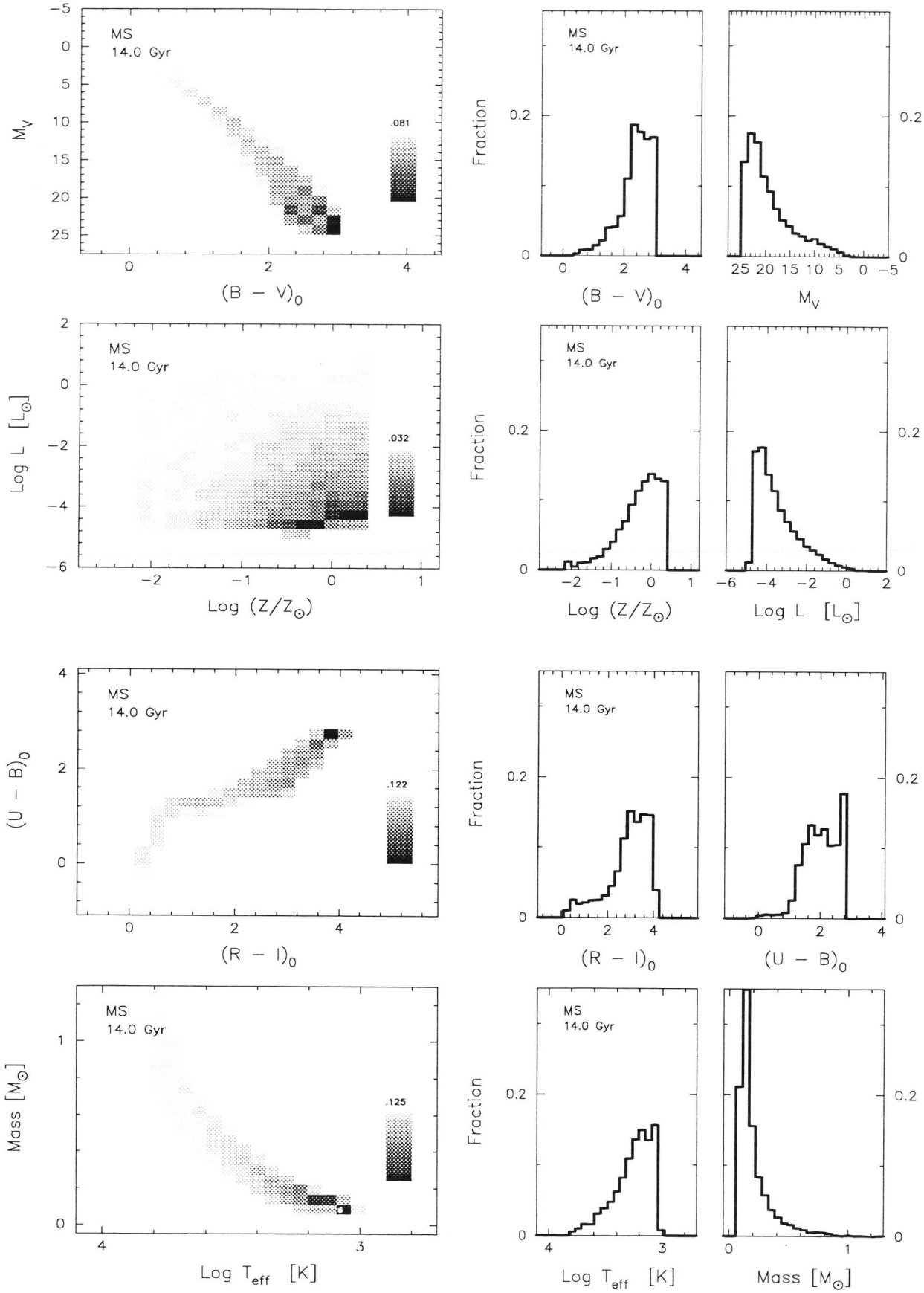

Figure 6.11 Resulting integrated properties of main-sequence stars at galactic age t_{ev} =14 Gyr in case of the exponentially decreasing SFR model (τ_{sfr} = 5 Gyr) ending at μ_1 = 0.1. A total of 10^4 main-sequence stars were selected according to the Salpeter IMF and SFR model adopted. Grey-scale corresponds to the fraction of all main-sequence stars selected within each bin (maximum bin content is indicated on top of legend).

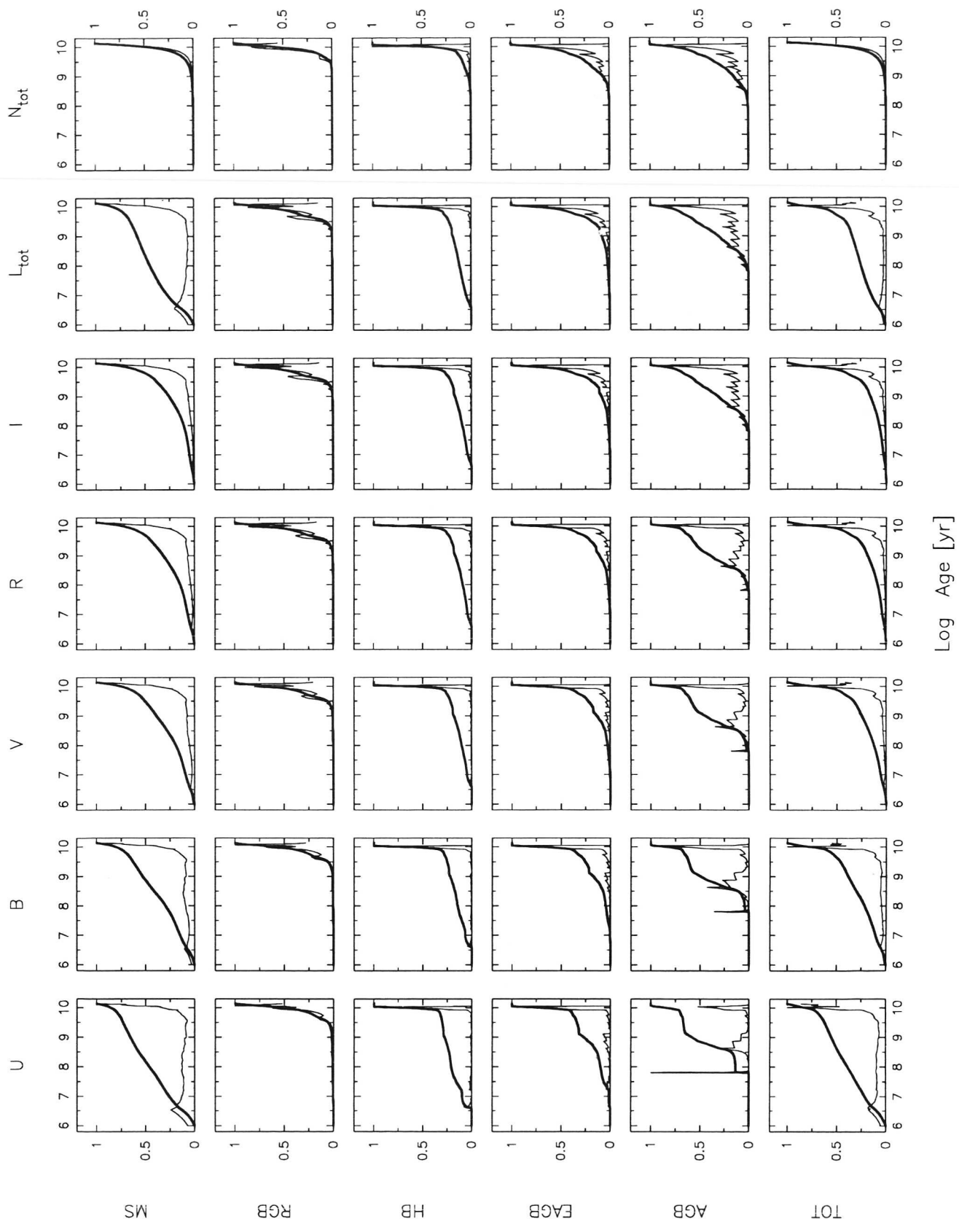

Figure 6.12 Resulting present-day luminosity (and number) contributions as a function of stellar age for stars in different evolutionary phases. Results are shown in case of the **exponentially decreasing SFR** model ($\tau_{\rm sfr} = 5$ Gyr) ending at $\mu_1 = 0.1$. Both normalised (*solid curve*) and cumulative (*thick solid*) distributions of (**left to right**) U, B, V, R, I, $L_{\rm tot}$, and $N_{\rm tot}$ are plotted for: (**top to bottom**) MS, RGB, HB, EAGB, AGB, and all (TOT) stars.

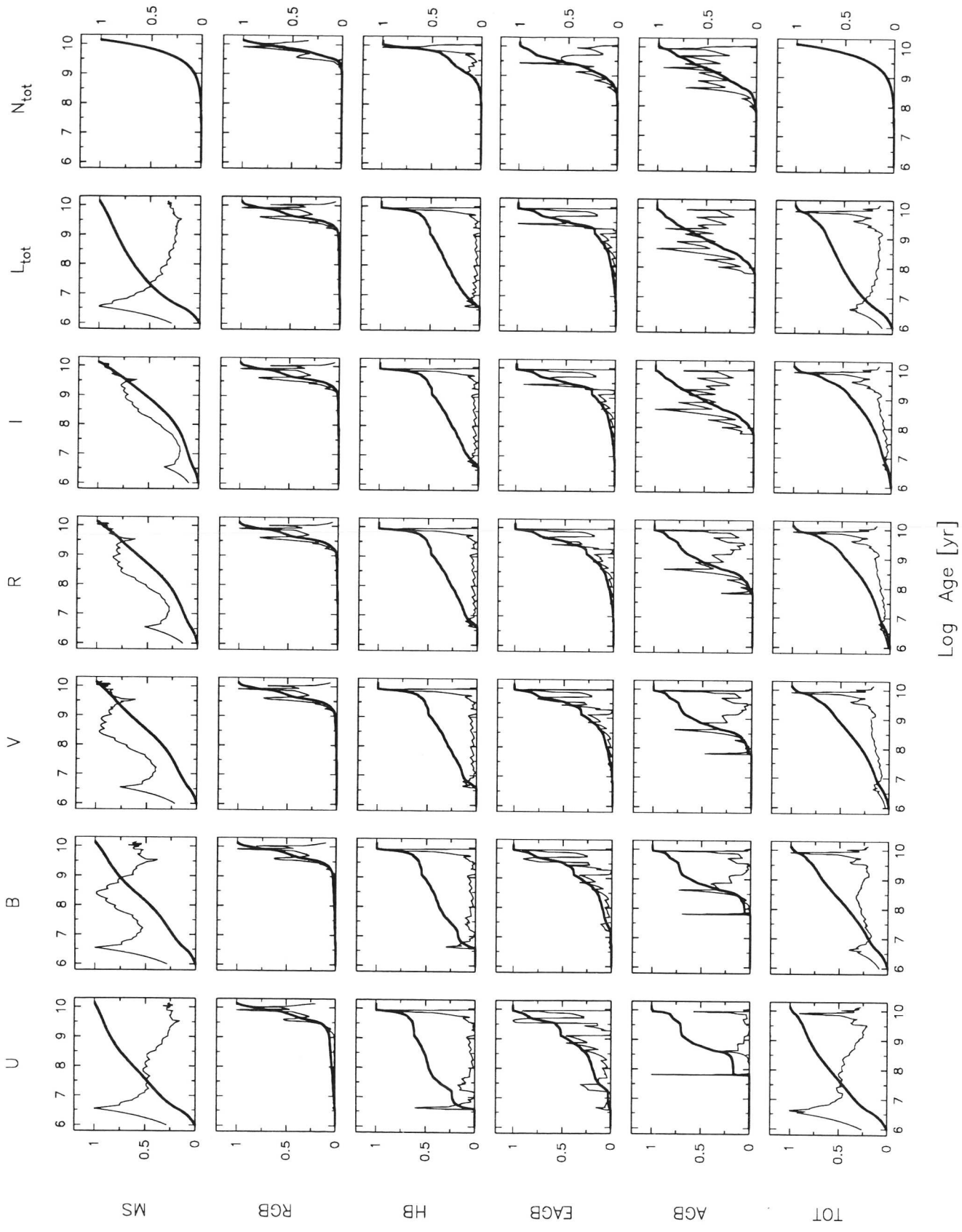

Figure 6.13 Resulting present-day luminosity and number contributions as a function of stellar age for stars in different evolutionary phases. Results are shown in case of the **constant SFR** model (τ_{sfr} = 5 Gyr) ending at μ_1 = 0.1. Both normalised (*solid curve*) and cumulative (*thick solid*) distributions of (**left to right**) U, B, V, R, I, L_{tot}, and N_{tot} are plotted for: (**top to bottom**) MS, RGB, HB, EAGB, AGB, and all (TOT) stars.

6.5 Results

We confront the basic set of star formation models discussed in the previous section with the complete set of observations available for LSB galaxies, including UBVRI broadband photometry, present-day HI masses, gas-to-total mass-ratios, and [O/H] abundances. We are primarily interested in global differences between the star formation history of LSB and HSB spirals. However, we attempt to extend some of our results to the sample of dwarf irregulars discussed in Sect. 6.2. In this section, we restrict ourselves to an investigation of model parameters related to the global galactic star formation history for a few standard SFR models. In the next sections, we consider the impact of small amplitude bursts on the photometric evolution of LSB galaxies and discuss what our results imply for each of the galaxy samples.

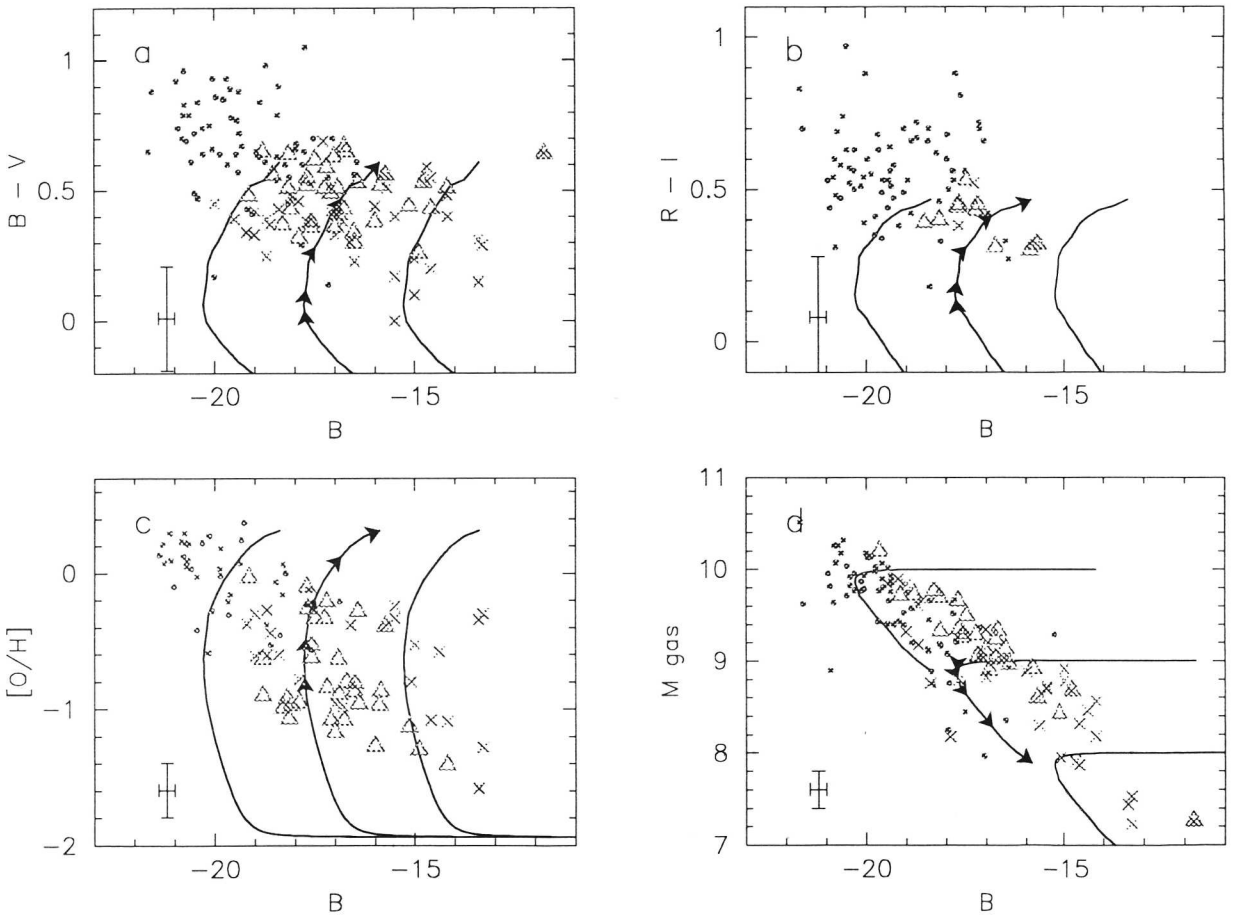

Figure 6.14 Exponentially decaying SFR model: photometric and chemical evolution results. Curves have been drawn for initial galaxy masses $M_g(t=0) = 10^8$, 10^9, and 10^{10} $M_\odot$. For the $M_g(t=0) = 10^9$ $M_\odot$ model, arrows indicate evolution times of 1, 2, 4, 8, and 14 Gyr, respectively, Symbols refer to the following galaxy samples: face-on HSB spirals (dots; de Jong & van der Kruit 1994), LSB spiral galaxies (triangles; de Blok et al. 1995), and dwarf irregulars (crosses; Melisse and Israel 1994). Typical observational errors are shown in the bottom left of each panel.

6.5.1 Star formation history of LSB vs. HSB galaxies

Predictions of exponentially decreasing SFR models are usually found in good agreement with observations of HSB galaxies with different *e-folding times for different Hubble types* (e.g. Larson & Tinsley 1978; Guiderdoni & Rocca-Volmerange 1987; Kennicutt 1989; Bruzual & Charlot 1993; Fritze-v. Alvensleben & Gerhard 1994).

In Fig. 6.14 we concentrate on the exponentially decreasing SFR model SFR$\propto \exp(-t/\tau_{\rm sfr})$ with $\tau_{\rm sfr}$ = 5 Gyr ending at a present-day gas-to-total mass-ratio of $\mu_1 = 0.1$ (appropriate to the Galactic disk; e.g. Clayton 1988). For this model, the chemical and spectro-photometric evolution have been followed during the last 14 Gyr. A value of $\mu_1 = 0.1$ was achieved by scaling the amplitude of the SFR accordingly. Model results are considered for the range of initial galaxy masses appropriate to LSB spirals, i.e. $M_g(t = 0) \sim$

$10^8 - 10^{10}$ $M_\odot$, in such a way that the ratio SFR(t=0) / $M_g(t = 0)$ remains constant. Note that galaxy colors and abundances are not affected by such scaling while, in contrast, absolute magnitudes and final gas masses scale with the adopted value of $M_g(t = 0)$ (as indicated by the distinct curves shown in each panel of Fig. 14).

LSB galaxies

Present-day (B−V) and (R−I) colors for the exponentially decreasing SFR model are 0.6 and 0.5 mag, respectively. These colors agree reasonably well with the *reddest* values observed for LSB galaxies. However, many LSB galaxies included in Fig. 6.14a exhibit present-day (B−V) colors $\lesssim 0.5$ mag that cannot be explained by the exponentially decreasing SFR model shown. The same appears true when considering the (R−I) colors (Fig. 6.14b) although these data are incomplete relative to the (B−V) data. Both the colors of (B−V) $\lesssim 0.5$ and (R−I) $\lesssim 0.4$ mag observed for many LSB galaxies indicate the presence of a bright stellar population probably younger than ∼5 Gyr (cf. Fig. 6.2). Alternatively, metallicity, extinction, IMF, and/or τ_{sfr} effects may play an important role in determining the (B−V) and (R−I) colors of LSB galaxies. We will discuss these possibilities further on in this paper.

Fig. 6.14c demonstrates that the [O/H] abundances predicted by the exponentially decaying SFR model are much larger than observed in LSB galaxies. Since current metal-abundances are primarily determined by the present-day gas-to-total mass-ratio μ_1, this is typical for SFR models ending at $\mu_1 = 0.1$ (cf. Table 6.3). The large range observed in [O/H] abundances at a given B magnitude (i.e. down to [O/H] = −1.4) indicates that substantial variations in stellar enrichment have occured among LSB galaxies. There are several plausible explanations for this: 1) LSB galaxies show present-day gas fractions much larger than $\mu_1 = 0.1$, 2) the ISM in LSB galaxies has been diluted by metal-poor material (e.g. by metal-deficient gas infall), 3) LSB galaxies exhibit a considerable range in age between 8 and 14 Gyr since the onset of main star formation in their disks, and/or 4) LSB galaxies experienced various degrees of stellar enrichment (e.g. due to differences in the IMF and/or quantities related to SNII enrichment). In the latter case, it would be necessary to explain why stellar enrichment in LSB galaxies would be distinct from that in HSB spirals for which exponentially decaying SFR models predict reasonable abundances (cf. Fig. 6.14c) assuming a Salpeter IMF and SNII enrichment as described Sect. 6.3.

Fig. 6.14d shows that exponentially decreasing SFR models ending at $\mu_1 = 0.1$ are also inconsistent with the total amount of gas $M_g \sim 1.4 M_{HI}$ (corrected for helium) observed in LSB galaxies of a given B magnitude, provided that the present amount of molecular gas in these systems is negligible (see Sect. 6.2). This is true for all SFR models in the case of $\mu_1 = 0.1$ (we exclude the possibility that LSB galaxies are younger than ∼ 1 Gyr; cf. Fig. 6.14d). These results imply that the present-day gas-to-total mass-ratios in LSB galaxies are much larger than $\mu_1 = 0.1$ and/or that substantial amounts of gas have been accreted in these systems during their evolution. Both possibilities are consistent with our findings from the [O/H] abundances. We conclude that exponentially decreasing SFR models ending at $\mu_1 = 0.1$ are inconsistent with the observed properties of LSB galaxies.

HSB galaxies

Present-day colors of HSB galaxies with (B−V)$\gtrsim$0.6 and (R−I)$\gtrsim$0.5 mag can be explained by the exponentially decreasing SFR model ending at $\mu_1 = 0.1$ only when substantial amounts of internal dust extinction are incorporated. The reason is that, even though a single stellar population born at Z=0.02 may become as red as (B−V)∼1.1 and (R−I)∼0.8 mag (cf. Fig. 6.2), the luminosity contribution by young stellar populations (with ages less than a few Gyr) results in substantial blueing of the galaxy colors. For the same reason, values of (B−V) $\gtrsim$ 0.65 mag are not predicted by our dust-free models independent of the adopted SFR or IMF (see below). Therefore, considerable reddening of, in particular, the emission associated with these *younger* stellar populations is required to explain the colors of HSB galaxies.

Since internal extinction in HSB galaxies up to E(B−V) ∼0.5 mag (corresponding to A_V ∼1.5 mag) is required, no matter what the detailed underlying star formation history of these systems is, extinction and metallicity may be one of the main explanations for the differences in color observed between LSB and HSB galaxies. This conclusion is consistent with the well established fact that most extinction in HSB galaxies originates from the galaxy nucleus and spiral arms (see Sect. 6.2), i.e. the sites where star formation and luminous young stellar populations in HSB galaxies are usually observed and which are weakly developed or absent in LSB galaxies. In this manner, LSB galaxies are not remarkably blue compared to HSB galaxies but instead the young stellar populations determining the colors of HSB galaxies appear exceptionally red due to relatively large amounts of internal extinction (and high metallicity). This view is consistent with independent arguments which suggest that reddening by dust in LSB galaxies is relatively unimportant (Sect. 6.2) and indicates that at least part of the color differences between HSB and LSB galaxies are due

to effects of extinction. We emphasize that the underlying stellar populations in LSB and HSB galaxies are distinctly different due to marked differences in the chemical evolution of these systems (see below). Therefore, extinction effects, although important, cannot be the entire explanation for the color differences observed.

Apart from extinction, reddening effects due to the inclusion of binaries and/or preferential formation of low mass stars may play a significant role in determining the colors of individual galaxies. Although a detailed investigation of these effects is beyond the scope of this paper, we have verified that reasonable corrections for binaries (by means of an enhanced contribution by post-MS stars) and for variations in the stellar IMF are unable to account for the observed color differences between LSB and HSB galaxies (even though such corrections can result in substantial reddening up to ~0.2 mag in (B−V) and ~0.15 mag in (R−I); cf. van den Hoek 1997).

Figs. 6.14c and d show that both the [O/H] abundance ratios and present-day gas masses of HSB galaxies can be explained reasonably well by exponentially decreasing SFR models ending at $\mu_1 \sim 0.1$ (provided that the upper HSB galaxies in Fig. 6.14d have initial masses as large as $M_g(t=0) \gtrsim 10^{11}$ $M_\odot$).

We conclude that, in contrast to LSB galaxies, exponentially decreasing SFR models ending at $\mu_1 = 0.1$ generally provide adequate explanations for the star formation history of late-type HSB galaxies when internal extinction is taken into account. This is consistent with the results from previous evolution models (with different stellar input data) for HSB galaxies (e.g. Larson & Tinsley 1978; Guiderdoni & Rocca-Volmerange 1987).

6.5.2 A more detailed comparison

In the previous section, we have argued that exponentially decreasing SFR models ending at a present-day gas-to-total mass-ratio $\mu_1 = 0.1$ are inconsistent with the observed B−V colors, abundances, gas fractions, and gas contents of LSB galaxies. We here extend the set of SFRs considered to models ending at values $\mu_1 = 0.025$, 0.1, 0.3, 0.5, 0.7, and 0.9, for the various star formation histories shown in Fig. 6.5.

Colors and magnitudes

Results for the exponentially decaying SFR models ending at values of $\mu_1 \gtrsim 0.025$ are shown in Fig. 6.15 (the amplitude of the SFR was scaled while maintaining the functional form of the SFR). While the age distribution of the stellar populations is the same for the models shown, present-day (B−V) and (R−I) colors are found to decrease by 0.2 and 0.1 mag, respectively, when going from models ending at $\mu_1 = 0.025$ to ~1 (cf. Figs. 6.15a,b). This blueing effect is due to the decrease of stellar initial metallicities for models ending at increasingly higher gas fractions. We emphasize that the abundance effect on the galaxy colors is substantial and originates from the metallicity dependent set of stellar evolution data used.

Exponentially decaying SFR models ending at values μ_1=0.5−0.7 are in best agreement with the (B−V) and (R−I) colors of a typical LSB galaxy with (B−V) ≳0.5 mag. Note that these results can be shifted towards brighter B magnitudes by assuming initial gas masses larger than $M_g(t = 0) = 10^{10}$ $M_\odot$ (and vice versa) while this leaves the resulting colors unaltered (cf. Fig. 6.14).

In principle, single burst SFR models in which all stars were formed about 5 Gyr ago with Z=0.001 predict colors of (B−V) = 0.55 and (R−I) = 0.4 mag that are consistent with the typical LSB galaxy colors observed as well (cf. Fig. 6.2). However, as recent star formation is observed in basically all the LSB galaxies in our sample (see below), a prominent stellar population much older than 5 Gyr must be present to compensate for the color contributions of the more recently formed stellar populations in these systems. Consequently, single burst models cannot be appropriate for the evolution of LSB galaxies and illustrate the need for roughly exponentially decreasing SFR models to fit the colors of LSB galaxies with (B−V) ≳0.5 mag.

In contrast, relatively blue LSB galaxies with (B−V) ≲0.4 mag cannot be fitted by exponentially decreasing SFR models *alone* (assuming t_{ev} = 14 Gyr), regardless of their current gas fraction μ_1. In these blue LSB galaxies a relatively young stellar population may contaminate the galaxy colors superimposed on an exponentially decreasing SFR. Alternatively, these LSB galaxies may be much younger than ~14 Gyr (e.g. 5−8 Gyr old, cf. Fig. 6.15a) and/or may have experienced linearly (i.e. more slowly than exponentially) decaying or constant SFRs which generally result in present-day colors of (B−V) ≲ 0.4 and (R−I) ≲ 0.35 mag.

This suggests that LSB galaxies can be distinguished in two major groups by means of their colors: one group with (B−V) ≳0.5 mag whose colors can be explained by exponentially decreasing SFR models (ending at t_{ev} = 14 Gyr) and a second group with (B−V) ≲0.5 mag which shows clear evidence for the

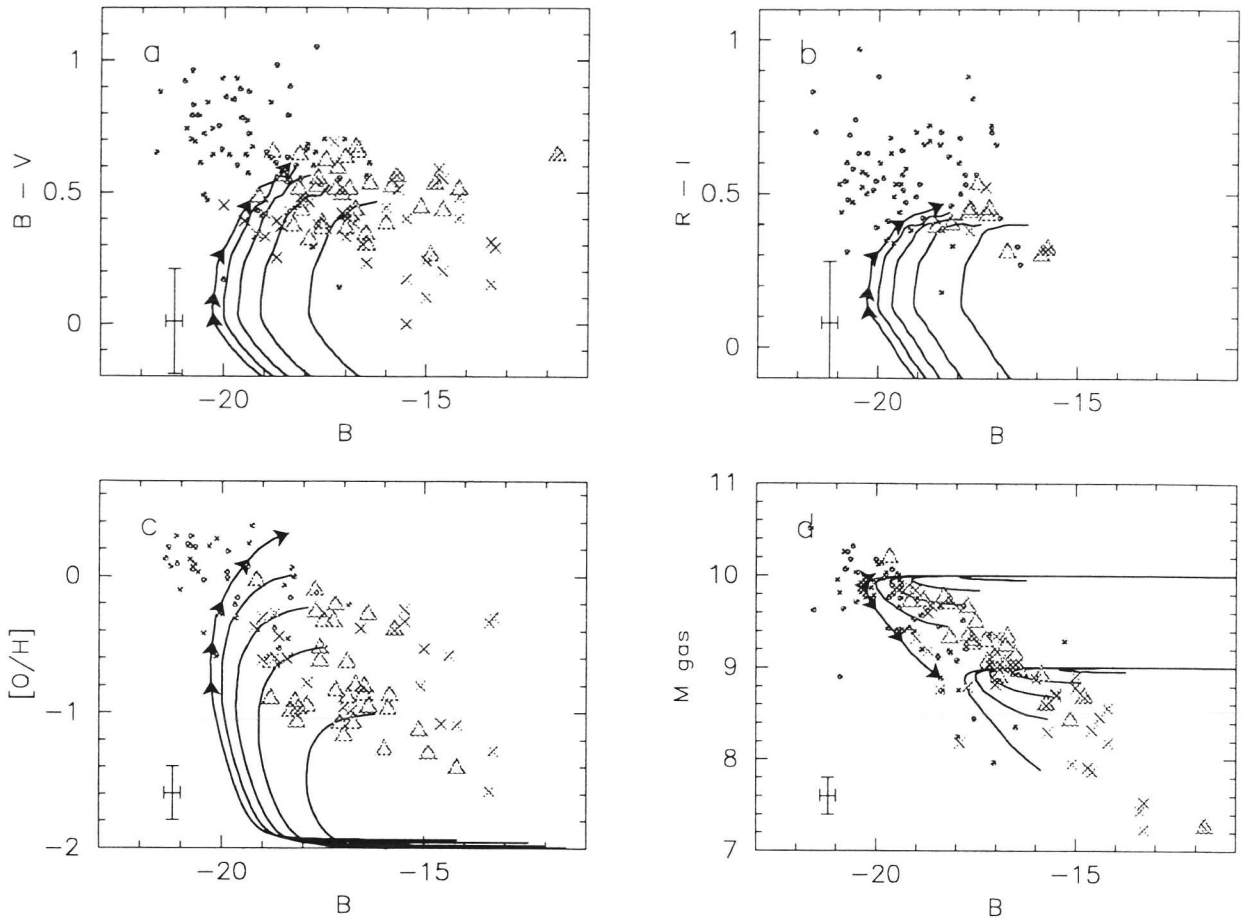

Figure 6.15 Photometric and chemical evolution results in case of exponentially decaying SFR models ending at μ_1 = 0.025, 0.3, 0.5, 0.7, and 0.9 for an initial galaxy mass of $M_g(t=0) = 10^{10}$ $M_\odot$ (in Fig. 6.15d we show also results for $M_g(t=0) = 10^9$ $M_\odot$). Arrows on top of the μ_1 = 0.025 model indicate evolution times of 1, 2, 4, 8, and 14 Gyr, respectively. Observational data as in Fig. 6.14

presence of a young stellar population that dominates the luminosity (e.g. these LSB galaxies may have: 1) experienced their onset of main star formation relatively recently, or 2) experienced a recent burst of star formation on top of an old stellar population; see Sect. 6.6).

Abundances

The observed range in [O/H] abundances for LSB galaxies is well explained by exponentially decaying SFR models with $\mu_1 \gtrsim 0.3$ (cf. Fig. 6.15c). However, constant SFR models ending at $\mu_1 \gtrsim 0.3$ are also consistent as the abundances of elements predominantly produced in massive stars are in general determined by the present-day gas fraction μ_1 and are insensitive to the detailed underlying star formation history (e.g. Tinsley 1980).

Metal-poor LSB galaxies with [O/H]$\lesssim -1$ probably have experienced low and sporadic star formation histories different from exponentially decaying or constant SFRs (low and constant SFRs appear to be excluded by the colors and gas fractions of these systems; see below). Alternatively, star formation may have turned on recently. In either case, such galaxies are relatively unevolved and usually have high gas-to-total mass-ratios. A substantial fraction of these metal-poor systems may have accreted considerable amounts of metal-poor gas since the onset of main star formation in their disks, maintaining the low abundances in the disk ISM (see Sect. 6.8).

Another effect which may play an important role for the enrichment of LSB galaxies is the stellar IMF. Although present observations are inconclusive, the very low gas surface densities observed in LSB galaxies may result in significantly lower low and high-mass cutoffs of the IMF, i.e. the preferential formation of low mass stars in LSB compared to that in HSB galaxies. For instance, a steep power law IMF with $\gamma = -3$ results in oxygen abundances of [O/H]$= -1$ at $\mu_1 = 0.1$ (cf. Table 6.3). On the other hand, steep IMF

models are unable to explain LSB galaxies with the highest relative luminosities and abundances, regardless of the assumed SFR history and value of μ_1, so that a range of IMFs would be needed to explain the entire range of abundances observed in LSB and HSB galaxies.

We estimate that at least ~30 % of the LSB galaxies in our sample have very low abundances (i.e. [O/H]$\lesssim -1$) with respect to their small present-day gas fractions (i.e. $\mu_1 \sim 0.5$) and probably experienced infall of substantial amounts of metal-poor gas and/or have formed stars relatively deficient in massive stars. We will return to these possibilities below.

Gas contents

Present-day gas masses observed in LSB galaxies can be well fitted by exponentially decaying SFR models ending at $\mu_1 = 0.3 - 0.5$ (note that the results can be shifted towards fainter B magnitudes and smaller present-day gas masses (and vice versa) by varying the adopted value for the initial mass $M_g(t = 0)$ while leaving predicted colors and abundances unaltered; cf. Fig. 6.15d). This is consistent with the range of $\mu_1 \gtrsim 0.3$ derived from the [O/H] data. Exponentially decreasing SFR models ending at $\mu_1 \gtrsim 0.6$ are clearly inconsistent with the observations if we exclude the possibility that LSB galaxies are extremely young systems with a stellar population younger than a few Gyr.

Present-day gas masses in combination with the colors and magnitudes observed in LSB galaxies, probably exclude e.g. constant or slowly decaying SFR models since such models predict present-day gas mass-to-light ratios that are too small compared to the observations (see below).

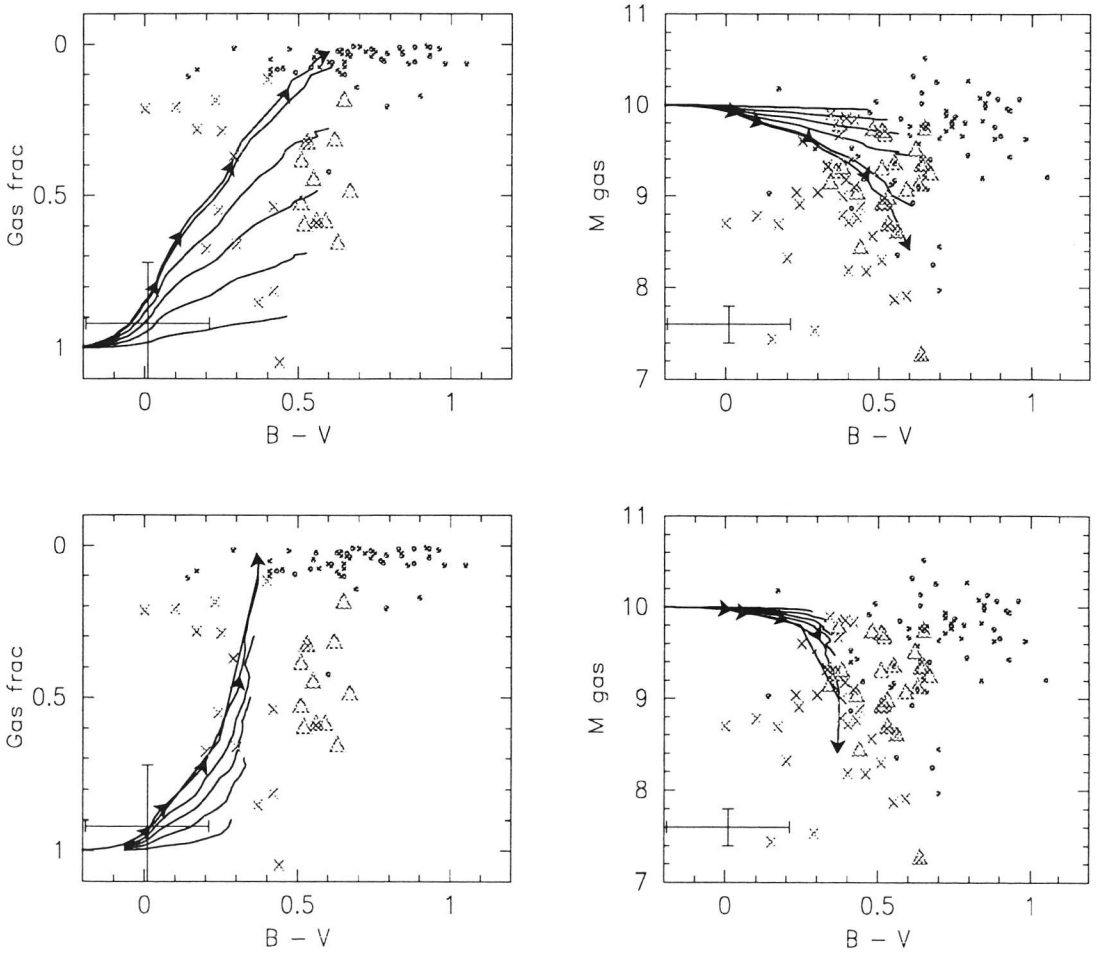

Figure 6.16 Comparison of model predicted and observed gas-to-total mass-ratios and total gas masses vs. (B−V). *Top panels:* exponentially decreasing SFR models. *Bottom panels:* constant SFR models. Models with SFR normalisations according to $\mu_1 = 0.025$, 0.1, 0.3, 0.5, 0.7, and 0.9 are shown for an initial galaxy mass of $M_g(t=0) = 10^{10}$ $M_\odot$. Arrows on top of the $\mu_1 = 0.025$ model indicate evolution times of 1, 2, 4, 8, and 14 Gyr, respectively. Observational data as in Fig. 6.14

Gas fractions

Fig. 6.16 displays the present-day gas-fraction and total amount of gas vs. (B−V) for constant and exponentially decaying SFR models. Exponentially decreasing SFR models are able to explain simultaneously values of $\mu_1 \sim 0.5 \pm 0.2$, (B−V)$\gtrsim$0.5 mag, and $M_g \gtrsim 10^9$ $M_\odot$, as observed for the majority of the LSB galaxies in our sample. Over the entire range of possible gas fractions, constant (or increasing) SFR models are clearly inconsistent with the observations provided that: 1) internal extinction in these galaxies is low (i.e. E(B−V) $\lesssim$ 0.1 mag; see Sect. 6.2.4), and 2) these galaxies have not recently accreted large amounts of gas, i.e. much larger than that presently observed within their optical disks. In fact, the inclusion of gas infall does not alter this conclusion since the colors predicted by such SFR models remain inconsistent with the observations.

For exponentially decreasing SFR models, we emphasize that (continuous) accretion of matter is consistent with the observations as long as: 1) the initial galaxy mass was substantially less than the typical dynamical mass $M_{dyn} = 10^{10}$ $M_\odot$ currently observed for LSB galaxies (see Table 6.1), and 2) a present-day gas fraction $\mu_1 = 0.5 \pm 0.2$ is predicted. Thus, the gas reservoir at the time of onset of main star formation in LSB galaxies may have been substantially less than that estimated from their present-day amounts of gas.

Similar conclusions can be reached when the gas mass-to-light ratio is considered (see below). Unfortunately, LSB galaxies for which reliable gas fractions are currently available are biased towards relatively red LSB galaxies with (B−V)$\gtrsim$ 0.5 mag. A few LSB galaxies with (B−V) $\lesssim$0.4 mag, however, may be best fitted by constant SFR models (or exponentially or more slowly decreasing SFR models with the contribution of an additional young stellar population superimposed).

Gas mass-to-light ratios

Fig. 6.17 demonstrates that exponentially decreasing SFR models ending at $\mu_1 \sim$0.5 are in good agreement with the observed atomic hydrogen mass-to-light ratios M_{HI} / L_B as well, in contrast to constant (or slowly decreasing) SFR models.

Consequently, our earlier finding that it is possible to distinguish the SFR history of LSB galaxies on the basis of their colors probably can be interpreted only in a manner consistent with their mass-to-light ratios, if most of the LSB galaxies with (B−V)$\lesssim$0.4 mag experienced exponentially (or somewhat less rapidly) decreasing SFRs with an additional luminosity and color contribution from a young stellar population. This finding essentially excludes constant SFR models for the majority of the LSB galaxies in our sample.

The high M_{HI} / L_B ratios and the large values of μ_1 observed for LSB galaxies can be interpreted in terms of slow evolution due to low rates of star formation and/or large amounts of gas infall since the onset of star formation. Infall would be consistent also with the relatively low abundances observed in some LSB galaxies with respect to their gas fractions.

As discussed in Sect. 6.2, the present-day gas fraction μ_1 used in this paper provides a hard lower limit to the actual gas-to-total mass-ratio within the optical radius of a LSB galaxy. In fact, the total amount of gas *available for star formation* within LSB galaxies may be much larger than that present within their optical radii. This may be due to accretion of matter from beyond their optical disk and/or infall of matter from large scale heights onto the disk. In either case, this would shift data points to the upper left in the M_{HI} / L_B vs. μ_1 diagram. However, from the agreement between the M_{HI} / L_B vs. (B−V) data observed and that predicted by exponentially decreasing SFR models ending at μ_1= 0.3−0.7 for the majority of the LSB galaxies in our sample, we argue that the observationally determined gas fractions of $\mu_1 \sim 0.5$ are probably accurate within ~50%. Some exceptions include the LSB and dwarf galaxies with M_{HI} / $L_B \gtrsim 2$ for which gas fractions of $\mu_1 \lesssim 0.5$ are likely underestimated by factors 2−3. This conclusion is insensitive to whether infall is involved or not (as long as μ_1= 0.3−0.7 and $M_{tot} \sim 10^{10}$ $M_\odot$ at present) but depends on our assumptions of $\tau_{sfr} = 5$ Gyr, $t_{ev} = 14$ Gyr, and E(B−V) $\lesssim$ 0.1 mag for LSB galaxies.

A possibility to reproduce the observed colors and M_{HI} / L_B ratios of LSB galaxies by constant or slowly decreasing SFR models would be if the contribution by post main-sequence stars to the galaxy integrated colors is considerably understimated in our models (e.g. due to IMF effects, binary inclusion, see Sect. 6.5.1). However, the predicted HI mass-to-light ratios for such models would lie far below those observed and large amounts of infall would be needed to compensate for this effect. Since the stellar evolution data used in our models is comparable to that of other recent photometric evolution models (see Sect. 6.4), a significant underestimate of the post-MS star contributions to the galaxy colors appears improbable. Therefore, it seems safe to conclude that constant and slowly (e.g. linearly) decreasing SFR models are appropriate only for a very small fraction ($\lesssim$10-15 %) of the LSB galaxies in our sample.

The main reason to conclude that constant and slowly decreasing SFR models are inconsistent with the observed photometric and chemical properties of LSB galaxies is based on the assumption of negligible amounts of dust extinction in these systems. However, if a considerable fraction of the LSB spirals in

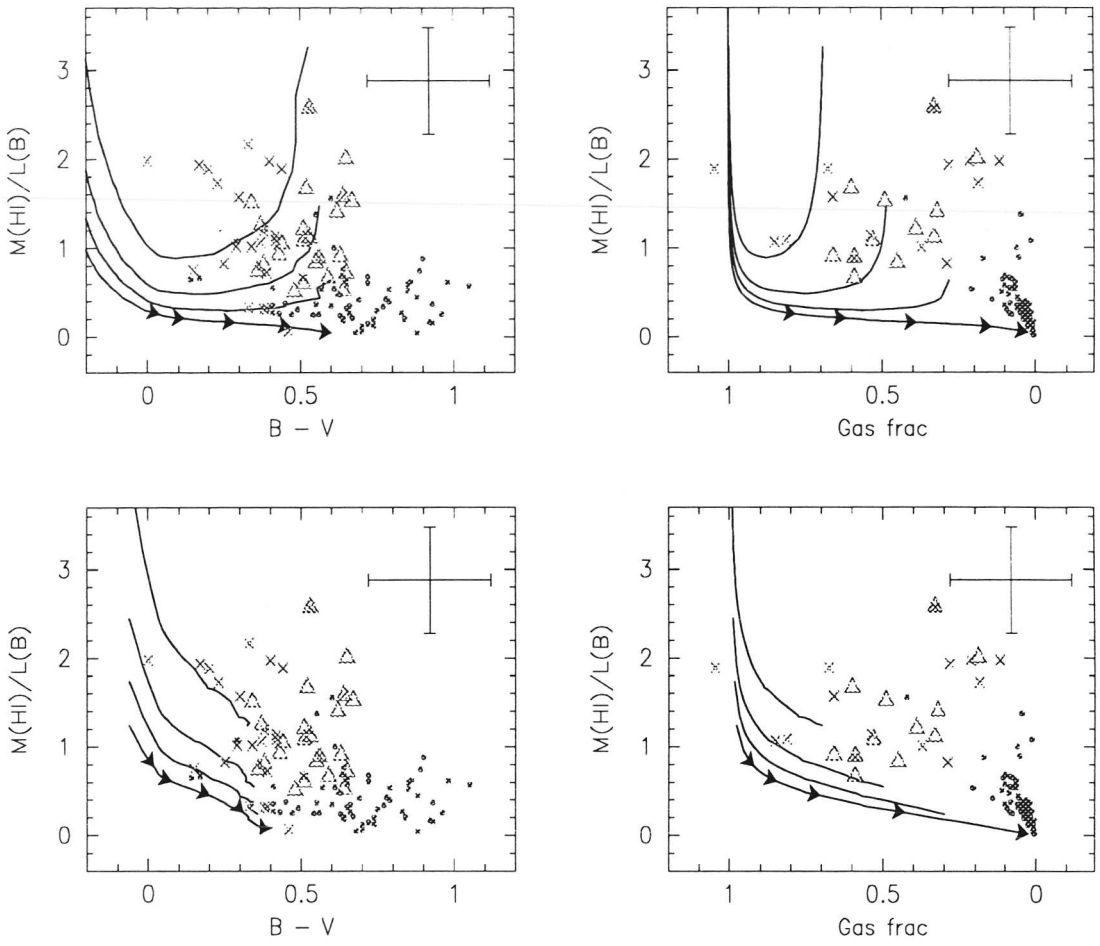

Figure 6.17 Evolution of M_{HI} / L_B vs. (B−V) (left) and M_{HI} / L_B vs. μ_1 (right). *Top panels:* exponentially decreasing SFR models, *bottom panels:* constant SFR models. From bottom to top, curves are shown for models ending at increasing gas fractions $\mu_1 = 0.1$, 0.3, 0.5, and 0.7, respectively. Arrows on top of the $\mu_1 = 0.1$ model indicate evolution times of 1, 2, 4, 8, and 14 Gyr, respectively. Observational data as in Fig. 6.16

our sample would suffer from extinctions of E(B−V) = 0.1 − 0.25 mag, the M_{HI} / L_B ratios predicted by constant SFR models would increase by a factor 1.4−2.5 after correction for internal extinction. In this manner, constant and slowly decreasing SFR models ending at gas fractions $\mu_1 = 0.3 - 0.7$ after ∼14 Gyr could also explain relatively red LSB galaxies with (B−V) $\gtrsim$ 0.5 mag and M_{HI} / L_B ratios as large as ∼1.5. However, we have argued in Sect. 6.2 that internal extinction in LSB galaxies is unlikely to exceed E(B−V)∼0.1 mag so that slowly decreasing and constant SFRs appear inconsistent with most of the LSB galaxies in our sample.

To summarize, we find that exponentially decreasing SFR models ending at $\mu_1 = 0.3 - 0.7$ are in optimal agreement with the colors, magnitudes, [O/H] abundances, gas contents, and mass-to-light ratios observed for LSB galaxies with (B−V) $\gtrsim$0.45 mag. For some of the LSB galaxies in our sample, the observed [O/H] abundances (as well as present-day gas contents) indicate that accretion of substantial amounts of metal-deficient gas has occured since the onset of star formation in their disks. Blue LSB galaxies with (B−V) $\lesssim$0.45 mag cannot be fitted by exponentially decreasing SFR models without an additional light contribution from a young stellar population. Alternatively, such LSB galaxies have experienced constant SFRs, SFRs more slowly decreasing than exponentially, or may be much younger than 14 Gyr. We presented arguments in favour of the possibility that such LSB galaxies experienced exponentially decreasing SFRs as well but with recent epochs of enhanced star formation. We will consider this possibility in more detail below.

6.6 Recent star formation in LSB galaxies

6.6.1 Luminosity contribution by H II regions in LSB galaxies

We investigate the contribution of young massive stars to the integrated colors and magnitudes of LSB galaxies. To this end, we select all HII regions that can be identified by eye, either from the Hα or R-band CCD images, and add up their total luminosity in a given passband. We define η_λ as the ratio of this HII region integrated luminosity and the luminosity of the hosting LSB galaxy. In this way, the brightest and largest HII regions within each LSB galaxy are easily traced although some HII regions may be missed due to extinction and selection effects (see below). The HII regions identified contain recently formed, massive OB stars that are hot and luminous enough to ionize the surrounding ISM.

Table 6.4 Observed broadband contributions by HII regions in LSB galaxies and derived SFRs

(1) Name	(2) #	(3) B mag	(4) I mag	(5) η_B	(6) η_I	(7) $(B-V)_{HII}$ mag	(8) $(B-V)_{gal}$ mag	(9) SFR^{cont}	(10) SFR^{burst} $[M_\odot\ yr^{-1}]$	(11) SFR^{tot}
F561-1	15	-14.4	-15.3	0.07	0.06	0.43	0.59	0.013	0.068	0.081
F563-1	12	-13.6	-14.1	0.05	0.12†	0.65	0.65	0.16	1.53	1.7†
F563-V1	4	-12.3	-13.6	0.04	0.04	0.53	0.56	0.005	0.019	0.024
F564-V3	16	-8.7	-10.1*	0.06	0.10*	0.78	0.64	–	–	–
F565-V2	4	-11.1	-12.2*	0.03	0.04*	0.72	0.53	0.017	0.055	0.072
F567-2	9	-14.3	-14.5	0.06	0.05†	0.90†	0.67	0.029	0.12	0.15
F568-1	4	-13.4	-14.7	0.02	0.02	0.41	0.62	0.12	0.19	0.31
F568-3	7	-14.5	-16.1	0.05	0.07	0.53	0.55	0.06	0.27	0.33
F568-V1	11	-15.4	-16.8	0.18	0.22	0.59	0.51	0.05	0.54	0.58
F571-5	10	-14.2	-14.6*	0.12	0.10*	0.28	0.34	–	–	–
F571-V1	5	-13.1	-13.9*	0.05	0.04*	0.40	0.53	0.033	0.11	0.14
F574-2	4	-13.3	-14.0*	0.03	0.03*	0.46	0.63	0.012	0.029	0.041
F577-V1	14	-15.7	-16.3*	0.18	0.19*	0.39	0.38	–	–	–
U128	17	-14.7	-16.2	0.04	0.06	0.55	0.51	0.14	0.68	0.82
U628	26	-15.7	-17.8	0.07	0.17	0.55	0.56	–	–	–
U1230	24	-14.7	-16.2	0.06	0.08	0.43	0.52	0.05	0.34	0.39

* values refer to R band magnitudes instead of I-band
† uncertain due to contamination by fore- or background objects
— μ_{rot} not determined

In columns (1) and (2) of Table 6.4, we list the LSB galaxy identification and number of HII regions selected. The number of HII regions identified within one LSB galaxy ranges from a few to ~25. For the ensemble of HII regions in each LSB galaxy, we tabulate the absolute B and I magnitudes as well as the corresponding ratios η_B and η_I of the HII region integrated luminosity and total LSB galaxy luminosity, in columns (3) to (6). Mean (B−V) colors for the HII regions and for the LSB galaxy as a whole are given in columns (7) and (8), respectively. Magnitudes and colours of the individual HII regions are found to vary over a wide range. This may be expected for HII regions differing in e.g. age, size, metallicity, IMF, etc. We find that there is a tendency of brighter magnitudes for LSB galaxies with larger number of identified HII regions. An exception is F564-V3 which is probably an extreme dwarf galaxy. We recall that the HII region integrated luminosity contribution may be strongly biased towards the properties of individual HII regions in LSB galaxies for which the total number of identified regions is low.

Substantial amounts of dust extinction within the HII regions in LSB galaxies are found to be present. First, (B−V) colors of many HII regions are nearly the same as (or even redder than) observed for the hosting LSB galaxy. Second, the HII regions identified are usually brighter in I than in the B band (cf. Table 6.4). Third, selective extinction of $E_{B-V} = 0.3\pm0.1$ mag is suggested by the reddening coefficients based on the ratio of Hα and Hβ lines towards the HII regions observed (e.g. McGaugh 1994; see also Osterbrock 1989). We note that a value of $E_{B-V} = 0.3$ mag is consistent with the typical extinction derived for HII regions in the Magellanic Clouds (e.g. Wilcots 1994). Also, very few HII regions display properties of an optically thin medium (McCall et al. 1985; Dopita & Evans 1986). Assuming a mean Galactic interstellar extinction curve, this corresponds to $A_B \sim 1.2\pm0.4$ and $A_I \sim 0.6\pm0.2$ mag. As the mean extinction curve for HII regions in low metallicity, low density LSB galaxies may be distinct from that in the Galactic disk, the actual extinction may be much lower.

For most of the LSB galaxies in our sample, the contribution by the HII regions to the total light emitted by LSB galaxies does not exceed $\eta = 0.05-0.1$ both in the B and I band. Corrected for extinction, the actual contributions may be larger, up to factors ~3–4 in B and ~2 in I, respectively, provided that the mean extinction in LSB galaxies is low compared to that in their constituent HII regions. Some HII regions may be missed due to dust extinction (values up to $E_{B-V} \sim 0.6-1.1$ mag are observed; e.g. McGaugh 1994) and/or seeing effects. Thus, the values of η_λ derived provide severe lower limits to the actual luminosity contributions of the HII regions.

For some LSB galaxies, e.g. F568-V1 and F577-V1, the HII region contribution is found as high as $\eta_\lambda = 0.2$ both in the B and I band. These systems contain a modest number of HII regions so that their HII regions on average may be larger and/or brighter than those present in several other LSB galaxies. Alternatively, the old stellar population within F568-V1 and F577-V1 may be under-represented due to a relatively low past SFR. This may apply in particular to F577-V1 which has (B–V)~0.4 mag and is among the bluest systems listed in Table 6.4.

Figure 12 shows the resulting HII region contributions η_λ in the B and I band for the SFR models discussed in Sect. 6.4. We assume a maximum age $\tau_{HII} = 5$ Myr for the HII regions observed in the LSB galaxies in our sample. This implies that stars more massive than ~25 $M_\odot$ are associated with the ionized regions identified in Hα, according to the stellar evolution tracks from the Geneva group (see below). Constant and increasing SFR models predict the HII region contribution η_λ to increase at recent epochs (both in the B and I bands). In contrast, exponentially decreasing SFR models predict η_λ to decrease. We note

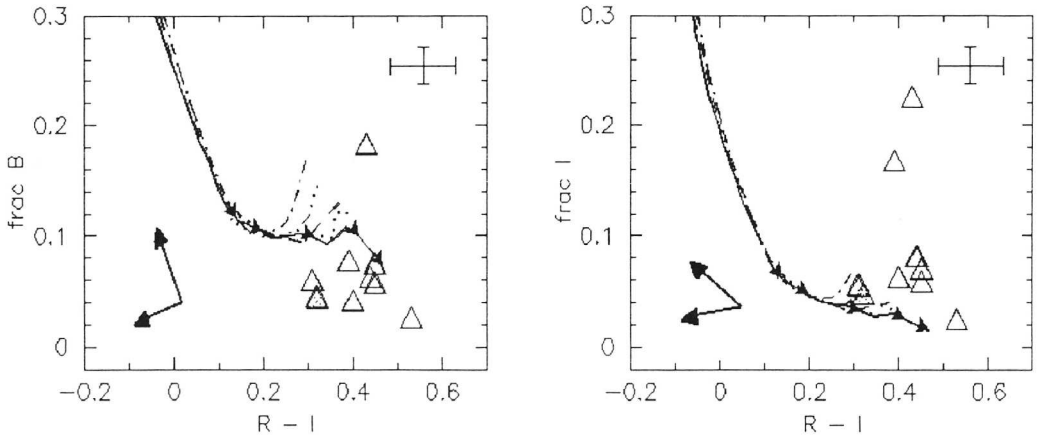

Figure 6.18 Evolution of the HII region integrated luminosity contribution for distinct SFR models ending at $\mu_1 = 0.1$. *Left panel:* Ratio of HII region integrated and total luminosity in the B band vs. (R–I). *Right panel:* same as left panel but for I band. For the exponentially decreasing SFR model, solid triangles indicate evolution times of 1, 2, 4, 8, and 14 Gyr, respectively. Observational data on LSB galaxies is shown as open triangles. Typical errors in the data (upper right) and directions to which the data would shift after corrections for extinction (bottom left) are indicated. Top and bottom arrows indicate corrections for extinction within the HII regions and the LSB galaxy, respectively

Corrections for dust extinction within the HII regions and LSB galaxy as a whole, respectively, will shift the observations in the directions as indicated in Fig. 6.18 (assuming a mean Galactic extinction curve). Clearly, the B band constributions by HII regions in LSB galaxies do not provide useful constraints on our models as extinction is too large at these wavelengths. However, from the I band observations we can conclude that the values of η_I predicted by smoothly varying SFR models are systematically too low by large factors for most of the LSB galaxies in our sample.

This is true in particular for F568-V1, F577-V1, and U628 for which values of $\eta_{I,R} \gtrsim 0.2-0.25$ suggest that star formation has been recently enhanced by factors ~5–10 relative to the SFRs predicted by exponentially decreasing or constant SFR models. Alternatively, the I band magnitudes of young stars used in our models may be considerably too low and/or the HII region lifetime assumed (i.e. $\tau_{HII} = 5$ Myr) may be too short. The former possibility can be excluded as synthetic color magnitude diagrams for young open clusters (e.g. V–I vs. I), based on the stellar evolution data adopted here, are in good agreement with the observations (van den Hoek 1997). The latter possibility can be excluded provided that stars older than ~20 Myr (i.e. initial mass $\lesssim$ 10 $M_\odot$) do not contribute substantially to the HII regions identified (see below). Thus, star formation may be recently enhanced in LSB galaxies with $\eta_{I,R} \gtrsim 0.2-0.25$.

As an additional check, we investigated whether there is a correlation between the HII region integrated contributions in the R band and M_{HI} / L. Such a correlation is expected when enhanced star formation is the primary cause for the high HII region contributions observed. Figure 6.19 shows that such a trend may be present, at least for the largest values of η_R observed. However, the data are affected by extinction and selection effects and additional observations are needed to be conclusive.

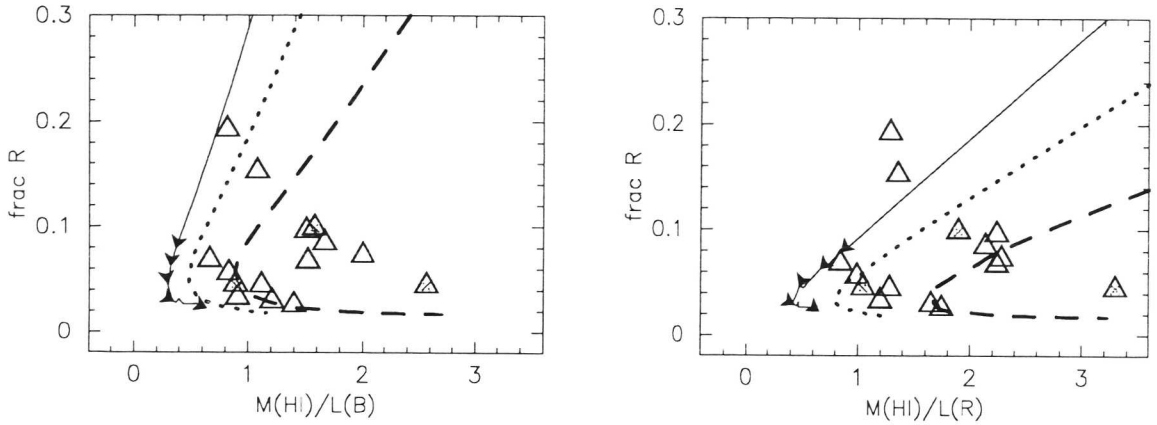

Figure 6.19 Evolution of the HII-region integrated luminosity contribution for exponentially decreasing SFR models. *Left panel:* Ratio of HII region integrated and total luminosity in the R band vs. M_{HI} / L_B for models ending at μ_1 = 0.3 (solid curve), 0.5 (dotted), and 0.7 (dashed). *Right panel:* same as left panel but vs. M_{HI} / L_R. Symbols have the same meaning as in Fig. 6.18.

We conclude that smoothly varying SFRs disagree with the observations. This is true in particular for the exponentially decreasing SFR models ending at $\mu_1 = 0.3-0.7$ which, as discussed in the previous section, are favoured for LSB galaxies. Note that models ending at gas fractions $\mu_1 > 0.1$ provide results similar to models ending at $\mu_1 = 0.1$ (i.e. the ratio of the young-to-old stellar luminosity contributions is independent of the normalisation of the SFR). We expect that LSB galaxies with high HII region contributions in the R and I band, such as F568-V1, F577-V1, and U628, are probably experiencing small amplitude bursts of star formation. Such bursts may be a common phenomenon in many LSB galaxies.

6.6.2 Effects of small amplitude star formation bursts

We investigate whether the large HII region integrated contributions to the galaxy integrated luminosity of $\eta_I \sim 0.25$ in the I band, as observed for several LSB galaxies discussed above, can be explained by small amplitude bursts of star formation.

We assume a Gaussian star formation burst profile with a given amplitude and width. The burst amplitude is taken as a free parameter which can be adjusted to fit the observations. To study the effect of the burst width (2σ), we consider burst durations Δt_b = 1, 5, and 10 Myr, respectively. For each burst profile we follow the chemical and photometric evolution during 1 Gyr with a time resolution of ~0.1 Myr at time of burst maximum and of ~2 Myr at roughly 5σ from burst maximum. We superimpose the star formation burst on each of the star formation models discussed in Sect. 6.5.1 while assuming a galactic evolution time at burst maximum of t_b = 13 Gyr, burst maximum amplitude A_b = 8 $M_\odot$ yr^{-1}, burst duration Δt_b = 5 Myr, maximum HII region lifetime τ_{HII} = 5 Myr, and an initial galaxy mass of 10^{10} $M_\odot$. In the following, we will refer to these burst parameters unless noted otherwise. For convenience, we neglect any influence of the burst on the chemical evolution of the model galaxy.

We show in Fig. 6.20a the resulting HII region integrated I band contribution η_I for an exponentially decreasing SFR plus burst model. Up to a galactic evolution time of ~13 Gyr the photometric evolution of the model galaxy is identical to that for the exponentially decreasing SFR model without burst (cf. Fig. 6.18). Thereafter, the contribution by young stars to the galactic integrated light increases rapidly. Simultaneously, the (R−I) colors become significantly bluer. After burst maximum, the contribution by young stars decreases and galaxy colors start to redden again until the effect of the burst becomes negligble and colors and magnitudes evolve as prior to the burst. We remark that the HII integrated-to-total luminosity ratio short after the burst can be substantially below those during the pre-burst evolution. This is due to the fact that stars somewhat older than τ_{HII} = 5 Myr dominate the galaxy light for a considerable time after the burst.

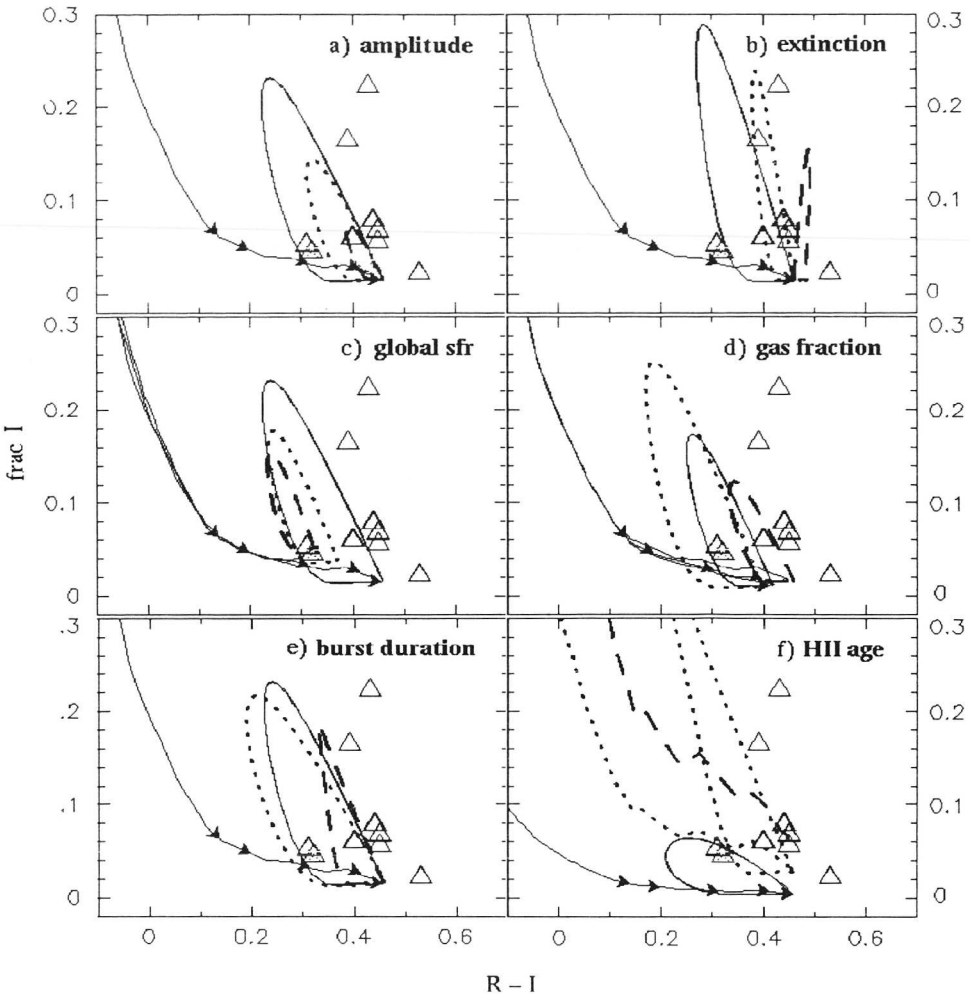

Figure 6.20 Impact of small amplitude bursts on the evolution of the HII region integrated luminosity contribution in the I-band vs. (R−I). Unless stated otherwise, we plot the exponentially decreasing SFR + burst model assuming $A_b = 8$ $M_\odot$ yr^{-1}, $\Delta t_b = 5$ Myr, $\tau_{HII} = 5$ Myr, and $E_{B-V} = 0$ mag. **a)** effect of varying burst amplitude: A_b [$M_\odot$ yr^{-1}] = 8 (solid curve), 4 (dotted), and 1.6 (dashed); **b)** effect of mean extinction within HII regions: E_{B-V} [mag] = 0.25 (solid curve), 0.5 (dotted), and 1 (dashed); **c)** effect of global star formation history: exponentially decreasing SFR (solid curve), constant (dotted), and linearly increasing (dashed); **d)** effect of actual gas-to-total mass ratio: $\mu_1 = 0.1$ (dashed curve), 0.5 (solid), and 0.7 (dotted); **e)** effect of burst duration: Δt_b [Myr] = 1 (dashed curve), 5 (solid), and 10 (dotted); **f)** effect of HII region age: τ_{HII} [Myr] = 2 (solid curve), 10 (dotted), and 50 (dashed; no burst shown). Symbols have the same meaning as in Fig. 6.18.

In this manner, a characteristic burst loop is completed as shown in Fig. 6.20a. The shape of this loop is determined by: a) the burst amplitude, b) the extinction within the HII regions, c)+d) the contribution by the old stellar population to the integrated galaxy light, e) the duration (and profile) of the burst, and f) the maximum lifetime of the HII regions during which young stars can be distinguished from the old stellar population. In addition, the IMF of the stars formed during the burst is of importance but we will argue that this effect is similar to that of varying the burst amplitude. Note that the shape of the burst loop is insensitive to the galactic age at which the burst occurs. This is because the contribution by young stars to the galaxy integrated colors change little over the past few Gyr for smoothly varying SFR models (cf. Fig. 6.18).

Burst amplitude and IMF: Fig. 6.20a demonstrates that high HII region integrated I band contributions $\eta_I \sim 0.25$ can be well explained by bursts with amplitude $A_b = 8$ $M_\odot$ yr^{-1} superimposed on an exponentially decreasing SFR model ending at $\mu_1 = 0.1$. Decreasing the burst amplitude by factors 2.5 and 5, respectively, results in the smaller loops shown in Fig. 6.20a. The actual burst amplitude required to explain the observations depends on many quantities as we will argue below.

The contribution by young stars to the galaxy integrated magnitudes and colors increases when considering burst IMFs that favour high mass star formation (e.g. m>10 M$_\odot$) compared to the Salpeter IMF. For various IMFs we find that the shape of the burst loop remains intact while the burst amplitude varies between 0.2 (steep IMFs; cf. Sect. 6.4.2) and 1.5 (Kroupa et al. IMF) normalised to 1 for the Salpeter IMF. Since high-mass stars dominate the HII region integrated luminosity contribution, the effect of varying the burst IMF is similar to that of varying the burst amplitude.

Dust extinction: Fig. 6.20b illustrates the effect of dust extinction in HII regions on the burst contribution to the I band luminosity as well as to the galaxy (R−I) color. A selective extinction of $E_{B-V} = 0.25$ (0.5) mag results in a reduction of the HII region integrated I band contribution by a factor 1.6 (2.5) and a reddening of $E_{R-I} = 0.14$ (0.27) mag, assuming a Galactic extinction curve. For values of $E_{B-V} \gtrsim 0.5$ mag, we find that the blueing effect on (R−I) by young massive stars formed during the burst is neutralized almost entirely by extinction. We note that a maximum extinction of $E_{B-V} \sim 1.1$ mag within the HII regions in LSB galaxies (e.g. McGaugh 1994) would result in a reduction in η_I by a factor ∼6.5 (for intense bursts even reddening of the galaxy colors may occur). If variations in the mean extinction of the ensembles of HII regions among LSB galaxies are small (e.g. less than a factor two), it is difficult to see how extinction alone can provide an adequate explanation for the large variations observed in η_I. We will return to this point below.

Global star formation history: Fig. 6.20c shows the impact of the assumed star formation history of the old stellar population on the effect of the burst. The burst effect on the galaxy magnitudes and colors increases when the contribution by the old stellar population is decreased. Thus, colors and magnitudes are less affected by bursts imposed on constant or even increasing SFRs compared to those imposed on exponentially decreasing SFR models: the smaller loop sizes just reflect that the mean age of the old stellar population is relatively young.

Current gas fraction: Fig. 6.20d demonstrates how the assumed present-day gas fraction μ_1 for an exponentially decreasing SFR model modifies the effect of the burst. The luminosity contribution by the old stellar population decreases for increasing values of μ_1. We find that the effect of a star formation burst for galaxies with $\mu_1 = 0.9$ (i.e. unevolved systems) is as large as that of a ten times stronger burst for $\mu_1 = 0.1$ (i.e. highly evolved systems). Thus, the burst amplitude required to explain the observations strongly depends on the present-day gas-to-total mass-ratio.

Burst duration: Fig. 6.20e shows that the duration of the burst affects the impact of the burst as well. For $\Delta t_b = 1$, 5, and 10 Myr, the variation in η_I is ∼0.25 while the resulting galaxy (R−I) colors become bluer. Burst durations in excess of $\Delta t_b \sim 5$ Myr are unlikely since this would require dust extinctions E(B−V) $\gtrsim$ 1 mag in order to provide agreement with the observed (R−I) colors. Such large extinction in HII regions are probably excluded by the observations (e.g. McGaugh 1994). Thus, relatively narrow burst profiles are needed to explain adequately extreme values $\eta_I \sim 0.2$ (as for F568-V1; cf. Table 6.4).

Maximum age of HII regions: Fig. 6.20f shows that when the maximum lifetime of the HII regions is increased from $\tau_{HII} = 5$ to 50 Myr, partial agreement with the observations can be achieved *without* invoking star formation bursts. Similarly, values of $\tau_{HII} \gtrsim 200$ Myr would be required to explain the large values of $\eta_I = 0.2$ observed (see below). We note that the resulting HII region contributions do not increase linearly with τ_{HII} as short lived massive stars dominate the luminosity contribution of all stars formed during the past τ_{HII} yr.

To explain the observed variations in η_I by means of variations in τ_{HII}, the question arises why such large variations would occur in the mean value of τ_{HII} among different LSB galaxies. First, this could be due to selection effects. In this case, fainter HII regions may be detected preferentially in regions of low surface brightness (e.g. the outer parts of LSB galaxies and/or LSB galaxies with relatively low surface brightnesses). We plot in Fig. 6.21 the average surface brightness of the HII regions within a given LSB galaxy vs. central surface brightness of the hosting LSB galaxy. Indeed there appears to be a trend of preferential detection of faint HII regions in LSB galaxies with low central surface brightnesses, but further observations are needed to clarify this interesting tendency.

Second, this could be due to physical effects. For instance, the formation of massive stars could be favoured in LSB galaxies with relatively high surface densities. Since fainter HII regions are probably ionized by less massive stars, as has been argued for HII regions in the Magellanic Clouds (e.g. Wilcots 1994), larger HII ages τ_{HII} may be associated with LSB galaxies having relatively low surface brightnesses (or equivalently low surface densities; cf. dB96). This would imply that systematic variations in the least massive star m_{ion} ionizing the HII regions are present from one LSB galaxy to another (consistent with the data shown in Fig.

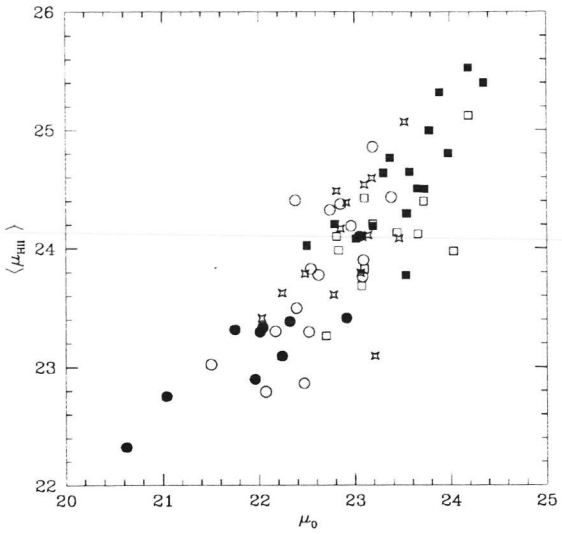

Figure 6.21 Mean surface brightness of HII regions vs. central surface brightness of the hosting LSB galaxy. Observational data refer to the U band (open squares), B (full squares), V (open stars), R (open circles), and I band (full circles)

6.21). This would be consistent with observations of sites of intense star formation which support the idea that the IMF is biased towards more massive stars in high surface density regions (e.g. Rieke & Lebofsky 1985).

Values of $\tau_{HII} \gtrsim 50$ Myr would mean that stars down to masses of $m_{ion} \lesssim 7$ $M_\odot$ would contribute to the HII regions identified (e.g. Schaerer et al. 1992; Z=0.001). Obervational estimates for m_{ion} are usually in the range 10−15 $M_\odot$ (Wilcots 1994; García-Vargas et al. 1995) and correspond to $\tau_{HII} \gtrsim 15$ Myr. Even though these values would imply that our adopted value of $\tau_{HII} = 5$ Myr is too low, this probably excludes extreme values of $\tau_{HII} = 200$ Myr which would be required to explain the observed range in η_I exclusively in terms of variations in τ_{HII} and/or m_{ion}.

Table 6.5 Effect of 5 Myr star burst model on galaxy magnitudes and colors for $M_g(0) = 10^{10}$ $M_\odot$

Model	A_b [$M_\odot$ yr^{-1}]	ΔB mag	ΔI mag	Δ(B−V) mag	Δ(R−I) mag	Notes
A1+burst	0.8	-0.34	-0.14	-0.18	-0.04	$SFR_1 = 0.17$ $M_\odot$ yr^{-1}
"	1.6	-0.58	-0.30	-0.28	-0.10	
"	3.0	-1.05	-0.42	-0.43	-0.17	*
"	8.0	-1.72	-0.53	-0.56	-0.26	*
B1+burst	0.8	-0.14	-0.06	-0.08	-0.02	$SFR_1 = 0.89$ $M_\odot$ yr^{-1}
"	1.6	-0.32	-0.21	-0.11	-0.07	
"	3.0	-0.56	-0.32	-0.21	-0.11	*
"	8.0	-0.94	-0.41	-0.33	-0.14	*

* E(B−V) $\gtrsim$ 0.3 mag in HII regions is required to provide agreement with observations

We conclude that variations in τ_{HII} (or equivalently m_{ion}) and/or extinction may provide an explanation only for part of the variations in the HII region integrated luminosity contributions observed among LSB galaxies. Therefore, the observations suggest that small amplitude bursts of star formation are important in at least several of the LSB galaxies for which accurate photometry data is available. Such recent episodes of enhanced star formation may play an important role in affecting the colors of the blue LSB galaxies discussed above.

6.6.3 Quantitative effect of small amplitude bursts on galaxy colors and magnitudes

Table 6.5 lists the effect of a 5 Myr star formation burst on the galaxy integrated magnitudes and colors for various burst amplitudes. For an exponentially decreasing SFR (model A1 in Table 6.3; assuming $M_g(0) = 10^{10}$ $M_\odot$, $\mu_1 = 0.1$, Salpeter IMF), we find that a burst with amplitude $A_b = 0.8$ $M_\odot$ yr^{-1} results in maximum color variations Δ(B−V) and Δ(R−I) of −0.18 and −0.04 mag, respectively. The effect of

increasing the burst amplitude by a factor ten to $A_b = 8$ $M_\odot$ yr^{-1} results in corresponding shifts of -0.56 and -0.26 mag, respectively. This effect is similar to that when the initial galaxy mass is reduced by a factor ten while leaving the burst amplitude unaltered. We note that exinction in HII regions is likely to suppress the color and magnitude effects of the bursts (i.e. the values given in Table 6.5 are hard upper limits).

For bursts superimposed on exponentially decreasing SFRs models ending at $\mu_1 = 0.1$, the color and magnitude shifts predicted are consistent with the observations in case of burst amplitudes $A_b \lesssim 3$ $M_\odot$ yr^{-1}, assuming a typical extinction of E(B−V) = 0.3 mag in the HII regions. In fact, the effect of the burst is determined mainly by the total luminosity of the young stellar populations formed according to the continuous SFR during e.g. the last Gyr. Since the amplitude of the SFR scales with (1- μ_1) for models ending at different gas fractions μ_1 (see Appendix B, Chap. 3), the impact of the burst for models ending at $\mu_1 = 0.5$ is about twice that given in Table 6.5. Similarly, for models ending at $\mu_1 \gtrsim 0.9$, the burst effect becomes roughly ten times stronger compared to the $\mu_1 = 0.1$ case (cf. Fig. 6.20).

We emphasize that the effect of the burst is substantially reduced when going from exponentially decreasing to constant SFRs (cf. Table 6.5). We will discuss in Sect. 6.8 how these results fit into a more general scenario for the star formation history of LSB galaxies.

Table 6.6 Observational estimates of present-day SFRs [$M_\odot$ yr^{-1}] in LSB galaxies*

(1) Name	(2) Dist. [Mpc]	(3) m_I	(4) R_I^{27} [kpc]	(5) R_{HI} [kpc]	(6) μ_I [arcsec^{-2}]	(7) M_{HI} [$M_\odot$]	(8) $<\sigma_{HI}>$ [$M_\odot$ pc^{-2}]	(9) SFR_1^{fix}	(10) SFR_1	(11) SFR^{cont}	(12) SFR^{tot}
F561-1	47	14.7	6.6	7.6	23.2	8.91	4.5	0.05	0.09	0.013	0.081
F563-1	34	16.1	10.2	16.3	26.4	9.19	1.0	(0.03)	(0.02)	0.16	1.7†
F563-V1	38	15.8	4.6	4.8	24.0	8.48	4.2	0.02	0.03	0.005	0.024
F567-2	56	15.9	8.4	10.6	24.6	9.09	3.5	0.04	0.06	0.029	0.15
F568-1	64	15.0	9.6	11.5	23.7	9.35	5.4	0.08	0.18	0.12	0.31
F568-3	58	14.7	8.7	11.4	23.3	9.20	3.9	0.09	0.14	0.06	0.33
F568-V1	60	15.7	8.4	10.7	24.3	9.14	3.8	0.05	0.07	0.05	0.58
U128	48	13.5	18.2	21.4	24.1	9.55	(2.0)	(0.16)	(0.21)	0.14	0.82
U1230	40	14.3	12.0	18.8	24.5	9.51	(4.3)	(0.11)	(0.15)	0.05	0.39

Notes: * theoretical values in columns (11) and (12) repeat those in columns (9) and (11) from Table 6.4; † probably contaminated by field galaxy; values between parentheses are uncertain.

6.7 Present-day star formation rates in LSB galaxies

6.7.1 Theoretical star formation rates

Global star formation rates are derived according to the best fitting models discussed in the previous section assuming an exponentially decreasing SFR, Salpeter IMF, and observational estimates for the current gas fraction μ_{rot} and total HI mass for each LSB galaxy individually according to:

$$SFR^{cont}\ [M_\odot yr^{-1}] \approx A(\mu_{rot})\ \frac{M^{tot}}{10^{10}} \qquad (6.3)$$

where $A(\mu_{rot})$ is the model SFR amplitude required to end at a gas fraction μ_{rot} at a galactic evolution time of 14 Gyr (assuming an initial mass of 10^{10} $M_\odot$) and M^{tot} the total galaxy mass as obtained from M_{HI} and μ_{rot}. We derived $A[M_\odot yr^{-1}] = 0.18$ ($\mu_{rot} = 0.1$), 0.13 (0.3), 0.09 (0.5), 0.06 (0.7), and 0.02 (0.9), respectively. Accordingly, we find that LSB galaxies show present-day SFRs (without bursts) between $SFR^{cont} \sim 0.01$ and 0.15 $M_\odot$ yr^{-1} (cf. Table 6.4). For a typical LSB galaxy (i.e. $M^{tot} = 10^{10}$ $M_\odot$, $\mu_{rot} = 0.5$) we estimate $SFR^{cont} = 0.1$ $M_\odot$ yr^{-1}.

The gas reservoir at the time of onset of main star formation in LSB galaxies may have been substantially less than that estimated from their present-day amounts of gas since infall and accretion of matter has probably been important in these galaxies. Furthermore, only part of the gas mass observed in LSB galaxies may be available for star formation. Therefore, we expect that the derived values of SFR^{cont} are upper limits to the continuum SFRs in LSB galaxies (within a factor 2–3). This remains true even while the total masses M^{tot} of LSB galaxies are underestimated by using the derived values of μ_{rot} (see Sect. 6.2).

As we discussed in Sect. 6.6, the effect of a starburst on the galaxy integrated magnitudes and colors depends on many quantities. Therefore, the amplitude of the star formation burst (superimposed on the exponentially decreasing SFR model) in best agreement with the observed values of η_λ is a rather uncertain

quantity (see Sect. 6.6). A detailed discussion of this problem is beyond the scope of this paper. However, assuming a modest HII region extinction of E(B−V) = 0.25 mag and lifetime $\tau_{\rm HII}$ = 20 Myr, crude estimates for the maximum burst amplitude can be derived from:

$$\mathrm{SFR^{burst}\ [M_\odot yr^{-1}]} \approx 20\eta_{\rm I}\ \frac{M_{\rm HI}}{10^{10}}\ \left(\frac{1}{\mu_{\rm rot}} - 1\right) \tag{6.4}$$

We find that I-band contributions of $\eta_{\rm I}$ = 0.2 are best explained by a 5 Myr burst with amplitude $\mathrm{SFR^{burst}}$ = 0.8 $\mathrm{M_\odot\ yr^{-1}}$, assuming present-day values of $\mathrm{M_{HI}}$ = 2 10^9 $\mathrm{M_\odot}$ and $\mu_{\rm rot}$ = 0.5.

Theoretical estimates for the total current SFRs in LSB galaxies are found from $\mathrm{SFR^{tot}}$ = $\mathrm{SFR^{cont}}$ + $\mathrm{SFR^{burst}}$ and are listed in the last two columns of Table 6.4. Present-day SFRs for LSB galaxies experiencing small amplitude bursts range from $\mathrm{SFR^{tot}} \sim 0.02$ to 0.8 $\mathrm{M_\odot\ yr^{-1}}$ (except for F563-1 for which the derived value of ∼1.7 $\mathrm{M_\odot\ yr^{-1}}$ is very unreliable). Concerning the uncertainties involved with e.g. the burst amplitude and current gas-to-total mass ratios, theoretical estimates for the actual SFR in each LSB galaxy probably lie between $\mathrm{SFR^{cont}}$ and $\mathrm{SFR^{tot}}$.

6.7.2 Empirical star formation rates

We have also derived current SFRs for LSB galaxies using the empirical method presented by Ryder & Dopita (1994; hereafter RD) based on CCD surface photometry of Galactic disks. These authors found an almost universal relationship between the Hα and I-band surface brightness *at a given radius* in the disks of a sample 34 of southern spiral galaxies. From this relation, RD derived a constraint on the present-day SFR integrated over the entire stellar mass spectrum as:

$$\log \mathrm{SFR_I[M_\odot pc^{-2} Gyr^{-1}]} = -0.26\mu_{\rm I} + 0.92 \log \sigma_{\rm HI} + 5.3 \tag{6.5}$$

where $\mu_{\rm I}$ is the I-band surface brightness and $\sigma_{\rm HI}$ is the global mean HI surface density [$\mathrm{M_\odot\ pc^{-2}}$] within the star-forming disk. The relation between $\mathrm{SFR_I}$ and $\mu_{\rm I}$ is normalised by a term related to the mean surface density $\sigma_{\rm HI}$ and by a constant which is partly related to the conversion of the massive star formation rate to total SFR depending on the adopted IMF (cf. Kennicutt 1983). It is unclear from the RD sample whether the relation is valid also for the lowest (stellar) I-band surface densities that are observed among LSB galaxies. However, since this relation holds over a wide range in surface brightness and massive star formation in the disks of spirals appears rather insensitive to galactic dynamics, extinction, and molecular gas content (RD), we expect this relation to be valid also in case of LSB galaxies. At the faintest surface brightnesses (i.e. $\mu_{\rm I} \gtrsim 25.6$ mag $\mathrm{arcsec^{-2}}$), the relation may be flattening off although the effects of sky subtraction and small number statistics leave this open to question. If flattening indeed occurs, Eq. (6.3) provides lower limits to the actual SFRs in LSB galaxies.

Using Eq. (6.1), we estimate global present-day SFRs for all LSB galaxies in our sample with measured I band magnitudes and related data. For these LSB galaxies we list the distance, apparent I band magnitude, and radius $\mathrm{R_{27}}$ at which the B band isophote is equal to 27 mag $\mathrm{arcsec^{-2}}$, in columns (2) to (4) in Table 6.6. This radius corresponds to the optical edge of the LSB galaxy and is more representative for the radius within which the old disk stellar population in LSB galaxies is contained than is $\mathrm{R_{25}}$ as used by RD for HSB galaxies. Accordingly, we define an effective I band surface brightness as:

$$\mu_{\rm I}^{\rm eff} = m_{\rm I} + 2.5 \log(\pi R_{27}^2) \tag{6.6}$$

and use this in Eq. (6.3). We tabulate the outermost radius of the measured HI rotation curve $\mathrm{R_{HI}}$, effective I band surface brightness $\mu_{\rm I}$ and total HI mass derived within $\mathrm{R_{HI}}$, and the mean global surface HI densities $\sigma_{\rm HI}$ in columns (5) to (8), respectively. The mean global HI surface densities $\sigma_{\rm HI}$ derived from these values range between 2 and 5.5 $\mathrm{M_\odot\ pc^{-2}}$ and are substantially smaller (i.e. by 20−60 %) than those derived using R_{27} instead. However, since $M_{\rm HI}$ has been measured within $R_{\rm HI}$, we expect the former values to be more representative of the average HI surface density in the star forming part of the disk.

The empirically derived mean present-day SFRs for the sample LSB galaxies range from about $\mathrm{SFR_I}$ = 0.02 to ∼0.2 $\mathrm{M_\odot\ yr^{-1}}$ (cf. column 10 of Table 6.6). Errors arising from the HI normalisation are estimated to be within a factor of two. This is illustrated when the same SFRs are derived assuming a fixed HI surface density of 2 $\mathrm{M_\odot\ pc^{-2}}$ for all LSB galaxies (cf. $\mathrm{SFR_I^{fix}}$ in Table 6.6). Other sources of errors include the conversion factor of massive-to-total SFRs as derived from the Hα luminosities (see Kennicutt 1983; RD) which may differ for HSB and LSB galaxies as this ratio is determined by the IMF and by theoretical estimates of the Hα radiation emitted by individual stars. For instance, the mean stellar population in LSB galaxies has a metallicity that is substantially lower than in HSB galaxies which will affect the stellar Hα emission. Probably the largest uncertainty arises from the possible flattening of the relationship between $\mu_{\rm H\alpha}$ and $\mu_{\rm I}$ found by RD towards low values of $\mu_{\rm I}$. We estimate that the *relative* SFRs for LSB galaxies

given in Table 6.6 are accurate within a factor of two while *absolute* SFRs may suffer from more substantial errors.

The empirically derived current SFRs in LSB galaxies range from $SFR_1 = 0.02$ to 0.2 $M_\odot$ yr^{-1}. This is in particularly good agreement with the theoretically derived SFRs ranging from SFR^{cont} ~0.01 to 0.15 $M_\odot$ yr^{-1} (cf. Table 6.6). As discussed before, the theoretically derived present-day SFRs of individual LSB galaxies lie probably between SFR^{cont} and SFR^{tot} where the latter values include the contribution of small amplitude bursts. In several cases, the values of SFR^{tot} are considerably larger than the empirical values which suggests that the burst contribution is overestimated by the models and/or that the SFRs derived empirically do not trace well local enhancements of star formation at the faint surface brightnesses of LSB galaxies. We conclude that the predicted SFRs in LSB galaxies generally agree to within a factor 2–3 with those derived empirically.

6.7.3 Comparison of present-day SFRs in LSB and HSB galaxies

We have derived current star formation rates in LSB galaxies of typically ~ 0.1 $M_\odot$ yr^{-1}. Several LSB galaxies in our sample are probably in a state of enhanced star formation and may experience small amplitude bursts of up to perhaps ~ 1 $M_\odot$ yr^{-1}. What fraction of the LSB galaxies actually is in such an excited state is difficult to estimate from current observations. In either case, the present-day SFRs in LSB galaxies are found considerably below the $\sim 5 - 10$ $M_\odot$ yr^{-1} derived for their HSB counterparts (e.g. Kennicutt 1992 and references therein) but significantly larger than the ~0.001 $M_\odot$ yr^{-1} observed tyically in dwarf irregular galaxies (e.g. Hunter & Gallagher 1986). Possible explanations for the marked differences in the present-day SFRs of LSB compared to HSB galaxies are discussed below.

6.8 Discussion

In the previous sections, we checked a comprehensive set of galactic photometric evolution models against a base of observations comprising the chemical and photometric properties of a representative sample of LSB galaxies. Here we discuss results of this comparison in the context of the early evolution and star formation history of such systems while focusing on the distinctly low evolutionary state of LSB relative to HSB galaxies.

6.8.1 Star formation history

For the majority of the LSB galaxies in our sample, observed UBVRI magnitudes, [O/H] abundances, gas masses and fractions, and HI mass-to-light ratios are best explained by galactic evolution models incorporating an exponentially decreasing global SFR ending at a present-day gas-to-total mass-ratio of $\mu_1 \sim 0.5$. When infall is involved to delay the chemical enrichment of the LSB galaxy disks, similar models ending at $\mu_1 \approx 0.3$ may be appropriate as well. When small amplitude bursts are involved to decrease the predicted M_g/L ratios, models ending at $\mu_1 \approx 0.7$ may also apply. In addition to exponentially decreasing SFR models, ~15% of the LSB galaxies require modest amounts of internal extinction $E(B-V) \lesssim 0.1$ mag to explain the relatively red colors of (B–V) ~0.6 mag of these systems.

A substantial fraction (~35 %) of the LSB galaxies in our sample have colors $(B-V) \lesssim 0.45$ mag which are inconsistently blue compared to the (B–V) colors predicted by exponentially decreasing global SFR models at galactic evolution times t_{ev} ~14 Gyr. Instead, these galaxies exhibit properties similar to those resulting from exponentially decreasing SFR models at evolution times of ~5–10 Gyr. Alternatively, recent episodes of enhanced star formation superimposed on exponentially decreasing SFR models may provide an adequate explanation for the colors of these systems (see Sect. 6.6). A small fraction of ~10–15 % of the LSB galaxies have properties (such as $(B-V) \lesssim 0.35$ mag) consistent with those resulting from slowly decreasing or constant SFR models ending at $\mu_1 = 0.5$. Although the current data are inconclusive to distinguish between the possibilities previously discussed, it is clear that the stellar population in these blue LSB galaxies must be relatively young.

Recent star formation is observed, at least at low levels, in essentially all the LSB galaxies in our sample. Hence, it seems justified to assume that the disks in LSB galaxies experienced continuous (i.e. frequent small amplitude bursts of) star formation, at least during the last few Gyr. Therefore, to explain the colors of LSB galaxies observed, the blue color contributions by stellar populations formed recently need to be compensated by the contributions of older stellar populations (provided that internal extinction is low; cf. Sect. 6.5.2). We have shown that star formation models which on average decay exponentially take such color compensation effects consistently into account. Thus, our result that these models are adequate for

most of the LSB galaxies in our sample basically relies on two assumptions: 1) negligible amounts of internal extinction, and 2) more or less continuous star formation in LSB galaxies.

Comparison with HSB and dwarf galaxies

The presence of an old stellar population in many late-type LSB galaxies as indicated by their optical colors (e.g. vdH93; dB95) and as confirmed by the results obtained in this paper suggests that LSB galaxies roughly follow the same evolutionary history as HSB galaxies, *except at a much lower rate.*

First, this suggests that the mean age of the stellar populations in most LSB and HSB galaxies is similar even though the disks of LSB galaxies are in a relatively low evolutionary state (see below). Although we cannot justify a uniform $\tau_{sfr} \sim 5$ Gyr for all LSB galaxies, our results indicate that, on average, the relative importance of the old (e.g. older than a few Gyr) and young stellar populations to the colors and luminosities of LSB galaxies are similar to that of late-type HSB galaxies. Values of $\tau_{\rm sfr} \ll 5$ Gyr would increase the colour contributions of the older stellar populations and would predict too red colors as compared to the colors observed for LSB galaxies. Such models probably can be excluded for LSB galaxies unless recent star formation in these systems would be more important than indicated by the observations. On the other hand, values of $\tau_{\rm sfr} \gg 5$ Gyr correspond to slowly decreasing or constant SFRs and would increase the colour contributions of the younger stellar populations. Such models would predict too blue colors and probably can be excluded for most of the LSB galaxies in our sample provided that extinction is low in these systems (i.e. E(B−V) $\lesssim$ 0.1 mag).

Secondly, this implies that the combined effect of extinction and metallicity on galaxy colors is sufficient to explain the color differences observed between LSB and HSB galaxies. Since the amount of extinction depends strongly on the dust content which in turn is determined by the heavy element abundances in the ISM (see Sect. 6.2), metallicity is probably the main quantity directing the color differences between LSB and HSB galaxies. In this manner, the much lower rate of star formation in LSB galaxies, which implies relatively low metallicities and dust contents, indirectly determines the blue colors of LSB galaxies compared to HSB galaxies.

Recent models indicate that the *stellar* surface density is probably a fundamental quantity in determining star formation in the disks of spiral galaxies (Dopita & Ryder 1994). Such models imply a roughly exponential decrease of the SFR with time for disk galaxies (Dopita 1985) and suggest that the initial onset of main star formation has been much more intense in HSB galaxies compared to LSB galaxies. Provided that star formation proceeds from the center outwards in disk galaxies (e.g. Burkert et al. 1994), this is consistent with the insignificant bulges observed in LSB galaxies. Our results discussed above are in good agreement with this scenario.

In summary, our results confirm that the properties of most late-type HSB galaxies can be best explained by exponentially decreasing SFR models ending at present-day gas fractions $\mu_1 \lesssim 0.05-0.1$ (see e.g. Clayton 1985; Dopita 1985; Guiderdoni & Rocca-Volmerange 1987). In contrast, LSB galaxies are best fitted by similar SFR models ending at $\mu_1 \gtrsim 0.3$. This implies that LSB galaxies must be in a low evolutionary state compared to HSB galaxies, a result which is consistent with the relatively blue colors, large gas fractions, high gas mass-to-light ratios, and low current star formation rates observed in LSB galaxies. Also, this is consistent with observations which indicate that, for a given total mass or luminosity, LSB galaxies usually have gas contents and gas-to-total mass-ratios much larger than their HSB counterparts of the same Hubble type (dB96). For instance, LSB galaxies are more gas-rich than the late-type spirals in the Virgo cluster (Cayatte et al. 1994). Furthermore, relatively low rates of evolution are indicated by the observational fact that LSB galaxies usually show properties comparable to those found in the outer parts of HSB spirals. In addition, the absence of the formation of grand design spiral arms in the disks of LSB galaxies is an indication of the low evolutionary state of LSB compared to HSB galaxies (Elmegreen 1990).

In the above discussion, we have treated the bulge-disk system as a whole when comparing LSB with HSB spirals. Clearly, a more detailed comparison should include radial variations of the galaxy properties. For instance, the bulges of LSB galaxies are much less prominent with respect to their disks than in HSB galaxies. What fraction of the current stellar content in LSB galaxies actually formed in their central parts is unclear but is an important issue when considering evolutionary differences between LSB galaxies and HSB galaxies in more detail (van den Hoek & de Blok, in preparation).

In general, there appears a trend along the Hubble sequence of rapidly decaying SFRs for early type galaxies, to constant or even increasing SFRs for dwarf irregular galaxies (see e.g. reviews by Sandage 1986; Kennicutt 1992). On average, the observed trend corresponds to a decrease of the ratio of mean past to present SFR along the Hubble sequence. Most of the LSB galaxies in our sample belong to the group of late-type Scd/Sd galaxies for which exponentially decreasing SFR models are in good agreement with the observations. The remaining LSB galaxies, for which slowly decreasing or constant (sporadic) SFR models

are more appropriate, belong to a group of galaxies with properties intermediate to those of disk galaxies with weak or absent spiral arms and Sm/Im galaxies. Thus, in general LSB galaxies comply well with the observed trend of SFR variation with Hubble type.

This picture is consistent with the finding that LSB galaxies usually cover the range of properties intermediate to that of HSB spirals and dwarf irregulars. Although not discussed in detail here, we have found that dwarf galaxies are best modelled using increasing or constant global SFR models. Since these systems are on average even bluer and usually have larger gas fractions than LSB galaxies, their rate of evolution must have been very low (e.g. Gallagher et al. 1984) while star formation probably has occured in bursts separated by quiescent periods in these systems (e.g. Searle & Sargent 1972; Sandage 1986; Hodge 1991; van Zee et al. 1996). In this case, the interburst period should be sufficiently long to allow young stars formed during the most recent burst to dominate the galaxy colors. To a lesser extent, the sporadic star formation scenario may apply to many of the LSB galaxies in our sample as well (cf. Sect. 6.6).

6.8.2 Present-day star formation

The presence of HII regions observed in virtually all the Hα images of the LSB galaxies in our sample suggest that recent star formation is a common phenomenon in these systems. The star formation sites in LSB galaxies generally do not trace the spiral arms and are preferentially found towards the edges of their optical disks. In particular, very little of the Hα emission is associated with the nuclei of LSB galaxies (which is in marked contrast with HSB galaxies).

We found evidence for the occurrence of small amplitude bursts in several LSB galaxies for which accurate data is available. This result indicates that current star formation in virtually all the LSB galaxies in our sample is *local* both in time and space and suggests that sporadic star formation has been a continuous process from the time star formation started in the disks of LSB galaxies.

The low star formation rates of $\sim$0.1 $M_\odot$ yr^{-1} derived for LSB galaxies as well as the local nature of the star formation in these systems are consistent with the idea of a critical threshold for the onset of global star formation in disk galaxies (e.g. Skillman 1987; Kennicutt 1989; Davies 1990). The mean star formation *threshold* as suggested from observations of irregular galaxies and spirals (Guiderdoni 1987; Kennicutt 1989) is about 8 $M_\odot$ pc^{-2}. This is slightly below the average HI peak surface densities of $\sim$8.7 $M_\odot$ pc^{-2} found for normal field Scd spirals (Warmels 1988; RD) and 10 $M_\odot$ pc^{-2} for Sd galaxies (Cayatte et al. 1994). In LSB galaxies, typical HI surface densities of $\sim$3 $M_\odot$ pc^{-2} are found (vdH93; cf. Table 6.6) which is well below the threshold. The idea of a star formation threshold is consistent with star formation models which state that star formation should increase with surface mass density (e.g. Dopita 1985; RD; see also Donas et al. 1987).

Even though LSB galaxies contain large amounts of gas, only very limited amounts participate in the process of star formation. If we assume that LSB galaxies maintain their current star formation rate of $\sim$0.1 $M_\odot$ yr^{-1}, their typical present-day amount of gas $\sim M_g = 2.5\ 10^9$ $M_\odot$ will be consumed within $\tau_{gas} = \sim$30 Gyr (for a recycled fraction of 25%). Such gas consumption times for LSB galaxies are much larger than a Hubble time (e.g. Romanishin 1980). For comparison, $\tau_{gas} \sim 2-4$ Gyr in HSB galaxies, assuming typically $M_g \sim 10^{10}$ $M_\odot$ and $SFR_I \sim 5$ $M_\odot$ yr^{-1}, which implies that HSB galaxies will run out of gas soon (see Kennicutt 1992).

Another reason for the low global star formation rates in LSB galaxies may be the fact that these systems are relatively isolated (Bothun et al. 1993) so that star formation is unlikely to be triggered by tidal interaction with nearby companions (e.g. Mo et al. 1994). Since the critical conditions for sporadic star formation can be reached only *locally* at the outer edges of the optical disks of LSB galaxies, this suggests that star formation may be associated with *local* accretion and/or infall of matter. This would naturally explain why the threshold can be reached in areas that are relatively void of stars and where the global gas surface density is relatively low.

The process of infall induced star formation is common in the Galactic disk (e.g. Lépine & Duvèrt 1994; van den Hoek & de Jong 1997) and may be the dominant mode of star formation in LSB galaxies in which low surface densities inhibit *global* star formation. In this manner, the LSB galaxies currently observed to undergo a small amplitude burst of star formation may have a relatively high gas infall rate.

The present-day star formation rates derived here for LSB galaxies place an upper limit on the gas infall rate in these systems of $\lesssim$0.3 ms yr^{-1}, provided that most of the infalling gas is associated with star formation. Such an infall rate would result in $\lesssim 4.5\ 10^9$ $M_\odot$ accreted in the form of gas over a disk lifetime of 14 Gyr and would imply that about half (up to all) of the total mass observed within the optical radius of LSB galaxies has been accreted and/or fallen in. More work is needed to settle the issue of gas infall and accretion in LSB galaxies.

Observations of gas-rich LSB galaxies and star-dominated HSB galaxies suggest that at least two star formation modes may be important in spiral galaxies: 1) a global, continuous star formation mode directed by accumulation of gas in the deep gravitational wells associated with old stellar population in the galactic nucleus and spiral arms (which basically involves the entire ISM on time scales of $\gtrsim$1 Gyr), and 2) a local, sporadic star formation mode associated with accretion and infall of matter interacting with gas already settled in the disk.

While the formation of low-mass stars (e.g. $m \lesssim 1$ $M_\odot$) may be primarily related to the *gas* surface density, the formation of high-mass stars may be related to the *total* (both gas and stellar) surface density. This results in a SFR depending both on the total surface density and surface density of the gas (see e.g. Dopita 1989; Dopita & Ryder 1995). The low surface densities in LSB galaxies may directly affect the IMF in the sense that formation of massive stars may be suppressed in these systems. Substantial variations in the massive star IMF observed in our own Galaxy (e.g. Garmany, Conti & Chiosi; 1982), e.g. may be related to variations in surface density. Furthermore, massive star formation in low surface density regions may temporarily inhibit (massive) star formation by controlling the pressure in the disk ISM and maintaining the vertical velocity dispersion (scale height) of the gas (e.g. Kennicutt 1989). Especially in LSB galaxies, this self-regulating mechanism of star formation may prevent the gas from reaching the critical surface density soon after star formation has occured. Observed differences between the star formation histories of the disks of LSB and HSB galaxies may be explained in terms of the relative importance of the high and low-mass star formation modes in these galaxies.

6.8.3 On the formation of LSB galaxies

Hierarchical theories of structure formation predict LSB galaxies to form at late times from small overdensities in the universe (Dalcanton et al. 1995). In this case, LSB galaxies form from the collapse of smaller amplitude overdensities than do HSB galaxies (Mo et al. 1994) since small amplitude peaks in the background density take longer to reach their maximum size and longer to recollapse than higher amplitude peaks. Furthermore, these small amplitude peaks are more likely to be found in underdense regions so that objects that collapse from small amplitude peaks will be less correlated than those that collapse from larger ones (Kaiser 1984; White et al. 1987). Another interesting prediction is that LSB galaxies should have lower *total* masses than HSB galaxies since low mass galaxies tend to form naturally with low surface densities according to hierarchical clustering theories.

This theoretical picture is consistent with observations which show that LSB galaxies are locally isolated systems (on scales $\lesssim$ 2 Mpc; e.g. Bothun et al. 1993) and that their separation weakly tends to increase towards fainter surface brightnesses (McGaugh, private communication). As the initial structure of galaxies can be strongly affected by their large-scale environments (Hoffman et al. 1992), the formation and low evolutionary state of LSB galaxies may be directed by their environment which favours long collapse times.

Several aspects concerning the formation and evolution of LSB galaxies have not been considered here. For instance, it is unclear whether large amounts of undetected gas are present in the haloes of LSB galaxies. In fact, the hydrogen mass in spirals may be underestimated by more than a factor 10 owing to the very inhomogeneous nature of cold molecular gas which, therefore, is difficult to detect (Pfenniger et al. 1994). Alternatively, this gas may be in the form of ionized hydrogen since protogalaxies with low column densities of gas may experience a delay in the recombination of ionized hydrogen until the extragalactic background flux has dropped below a certain value (Babul & Rees 1992). This prevents star formation over large scales in these galaxies (Corbelli & Salpeter 1996).

The presence of large amounts of dark matter in the haloes of LSB galaxies compared to that in HSB galaxies is strongly suggested by the rotation curves of these systems (dB96). It is found that LSB galaxies do not only have diffuse disks but are diffuse also in their distribution of dark matter. If the dark matter ultimately turns out to be gas, this would strongly suggest that large amounts of dark matter are still to be accreted and converted into stars within LSB galaxies, implying that these systems will ultimately end as HSB galaxies.

6.9 Concluding remarks

The reason why LSB galaxies can maintain their gas surface densities below the star formation threshold for very long times is probably related to the settling of their disks and the onset of star formation therein. In fact, LSB galaxies may evolve at a low rate because they are relatively isolated systems (e.g. Bothun et al. 1993) and their disk gravitational potentials are relatively weak. Observations indicate that LSB galaxies are very extended compared to HSB galaxies and that LSB galaxies have truly low matter densities both

in their disks and haloes (dB96) which implies slow contraction and accretion of matter. Furthermore, the large total gas masses and low rotation velocities suggest that LSB galaxies are still in the process of galaxy formation.

The inconspicuous spiral arms in LSB galaxies may be related to their low surface densities and/or to their low rotation velocities in combination with the gradual formation of their disks. Since there appear to be no HSB galaxies with weakly developed spiral arms, low surface brightness may imply weakly developed spiral arms. In addition, high rates of gas accretion over long evolution times may be required to form and maintain pronounced spiral structure.

Recent theories of galaxy formation predict that continuous infall is very important in the outer parts of disk galaxies over long evolution times (e.g. Gunn 1987; Steinmetz & Müller 1995). In this manner, galaxies continue to build up during their evolution instead of being formed at one preferred epoch. This is probably true for LSB galaxies which contain large fractions of their total atomic hydrogen content beyond the edges of their optical disks and perhaps also beyond the outermost points of their rotation curves measured. This implies intrinsic age differences between the gaseous disks of LSB and HSB galaxies even though the mean age of the stellar populations formed in these disks may be similar.

From theoretical computations it has been found that the formation time scale of Galactic disks strongly depends on the surface density (Burkert et al. 1992) which implies that the disk forms from inside out and that star formation progresses outwards in the disk. In particular, infall time scales are much longer at the outer radii of the gaseous disk (e.g. Larson 1976) while the inner disk depletes gas at short time scales. This is consistent with the fact that the major portion of the HI lies outside the star forming disk in many late-type disk galaxies (e.g. Kennicutt 1992; dB96). The low surface densities in the extended disks of LSB galaxies enable long dynamical time scales so that LSB galaxies are likely to represent an early stage of disk formation in which large amounts of gas are left-over after the initial collapse (i.e. with respect to that in HSB galaxies).

This picture is consistent with observations which show that the outer parts of LSB galaxies are usually bluer than their inner parts (which appear more evolved; e.g. van der Hulst et al. 1987; Bothun et al. 1990; Knezek 1993). Furthermore, color gradients in LSB galaxies are generally large compared to those in HSB galaxies (e.g. de Jong 1995; dB95) which is consistent with the low evolutionary state of LSB compared to HSB galaxies.

Overall, the low evolutionary state of LSB galaxies relative to HSB galaxies suggests that LSB galaxies are just HSB galaxies in the making (except on time scales much longer than a Hubble time). The low evolutionary state of LSB galaxies as confirmed by the results in this paper indicates that the process of collapse and secular contraction of the disk is still going on and proceeds in a regular fashion. Since LSB galaxies probably formed in relatively low density regions of the universe, infall and accretion of matter from their primordial gas reservoir is likely to play a major role in the evolution of their disks.

In the near future, near-IR observations will provide valuable information tracing the old red, metal-poor stellar population in LSB galaxies. Also, extension of the LSB galaxy observations towards smaller HI contents and lower HI surface densities will be very useful. In addition, many LSB galaxies may be still undetected at the faint end of the galaxy luminosity function (i.e. fainter than $B \sim -15$ mag). Such observations surely will provide many new insights concerning the evolution of low surface brightness galaxies.

Acknowledgements

We thank Andre Maeder and Georges Meynet for providing us with the stellar isochrone data and conversion programs. We thank Roelof de Jong for making available to us the data of a large sample of face-on spirals. We are grateful to the referee Dr. Uta Fritze–von Alvensleben for constructive comments from which this paper has benefitted.